



# Triple-functional polyetheretherketone surface with enhanced bacteriostasis and anti-inflammatory and osseointegrative properties for implant application



Xiao Xu<sup>a</sup>, Yongliang Li<sup>b</sup>, Lixin Wang<sup>c</sup>, Yan Li<sup>d</sup>, Jijia Pan<sup>d</sup>, Xiaoming Fu<sup>a</sup>, Zuyuan Luo<sup>d</sup>, Yi Sui<sup>a</sup>, Siqu Zhang<sup>d</sup>, Liang Wang<sup>a</sup>, Yaofeng Ni<sup>c</sup>, Lei Zhang<sup>a,\*\*</sup>, Shicheng Wei<sup>a,d,\*</sup>

<sup>a</sup> Department of Oral and Maxillofacial Surgery/Central Laboratory, Peking University School and Hospital of Stomatology, National Engineering Laboratory for Digital and Material Technology of Stomatology, Beijing Key Laboratory of Digital Stomatology, Beijing 100081, PR China

<sup>b</sup> Second Dental Center, School and Hospital of Stomatology, Peking University, Beijing 100081, PR China

<sup>c</sup> Department of Stomatology, Beijing Shijitan Hospital, Capital Medical University, Beijing 100038, PR China

<sup>d</sup> Laboratory of Biomaterials and Regenerative Medicine, Academy for Advanced Interdisciplinary Studies, Peking University, Beijing 100871, PR China

## ARTICLE INFO

### Keywords:

Bacteriostasis  
anti-inflammation  
osseointegration  
PEEK  
Dex/Mino liposomes

## ABSTRACT

Polyetheretherketone (PEEK) is considered a potential orthopedic/dental material because of its excellent mechanical and chemical properties (e.g., similar elastic modulus to that of human bone). However, the poor bacteriostasis and anti-inflammatory and osseointegrative properties of bioinert PEEK impede its clinical application. We previously developed a facile and versatile surface modification method using dexamethasone plus minocycline-loaded liposomes (Dex/Mino liposomes) bonded by a mussel-inspired polydopamine coating, which effectively modulated cell inflammatory response and discouraged bacterial colonization *in vitro*. Herein, we report the application of this multifunctional surface modification method to improve bioinert PEEK, aimed at further studying the *in vitro* osteogenesis and *in vivo* properties of Dex/Mino liposome-modified PEEK to prevent bacterial contamination, attenuate the inflammatory response, and enhance ossification for physiologic osseointegration. Our study established that the Dex/Mino liposome-modified PEEK surface presented favorable stability and cytocompatibility. Compared with bare PEEK, improved osteogenic differentiation of human mesenchymal stem cells under both osteoinductive and osteoconductive conditions was found on the functionalized surface due to the liposomal Dex releasing. *In vivo* bacteriostasis assay confirmed that Mino released from the functionalized surface provided an effective antibacterial effect. Moreover, the subcutaneous foreign body reaction and beagle femur implantation models corroborated the enhanced anti-inflammatory and osseointegrative properties of the functionalized PEEK. Our findings indicate that the developed Dex/Mino liposome-modified PEEK with enhanced antibacterial, anti-inflammatory, and osseointegrative capacity has great potential as an orthopedic/dental implant material for clinical application.

## 1. Introduction

Orthopedic/dental implants are common hard-tissue substitutes for remediless bone destruction [1,2]. Various properties of polyetheretherketone (PEEK) suggest it as a potential substitute for traditional metallic biomedical implants [3,4]. Compared with traditional metals, PEEK has a lower elastic modulus that is close to that of human cortical bone. This similarity can reduce the stress shielding effect caused by elasticity mismatch, avoiding possible bone lesions [5–7].

Additionally, PEEK endows natural radiolucency, excellent mechanical properties, and chemical resistance [8]. Despite these advantages, regrettably, the bioinertia of PEEK leads to poor bioactivity and impedes its osseointegration after implantation [9–11].

Osseointegration is a process involving the formation of a direct bone-to-implant contact without intervening fibrous connective tissue, providing an ordered and persistent functional connection for the implantation [12]. As a determining factor of successful bone regeneration, osseointegration is critical for initially stable anchorage and long-

\* Corresponding author. Department of Oral and Maxillofacial Surgery/Central Laboratory, Peking University School and Hospital of Stomatology, National Engineering Laboratory for Digital and Material Technology of Stomatology, Beijing Key Laboratory of Digital Stomatology, Beijing 100081, PR China

\*\* Corresponding author. Department of Oral and Maxillofacial Surgery, Peking University School and Hospital of Stomatology, Beijing 100081, PR China.

E-mail addresses: [zhlei\\_doctor@sina.com](mailto:zhlei_doctor@sina.com) (L. Zhang), [sc-wei@pku.edu.cn](mailto:sc-wei@pku.edu.cn) (S. Wei).

<https://doi.org/10.1016/j.biomaterials.2019.05.014>

Received 6 December 2018; Received in revised form 8 May 2019; Accepted 8 May 2019

Available online 11 May 2019

0142-9612/ © 2019 Elsevier Ltd. All rights reserved.

term functionalization of implants [13]. However, unsuccessful osseointegration may result in an increased risk of loosening and, eventually, complete failure of implants [14,15]. One of the risk factors for inferior osseointegration is implant surface contamination, which is a process triggered rapidly by initial bacteria adhesion to subsequent biofilm formation [16]. Oral infection and neighboring tissue destruction could be caused by a reduction of bacteriostasis at the implant–tissue interface, consequently leading to implant loosening and eventual detachment [17,18]. As well as bacterial infection, the host's foreign body reaction triggered by implants is another obstacle to its osseointegration [19]. Upon implantation, implants can evoke foreign body response at the implant–tissue interface, which is characterized by infiltration of numerous inflammatory cells and, eventually, encapsulation of the implants by dense fibrotic tissue, leading to failure of the implants [20,21]. It is well-known that the bioactivity of an implant itself, and its surface, are crucial factors for implant success; a lack of bioactivity (especially osteogenic capacity) can result in poor osseointegration [22]. For example, the inert PEEK has no bioactivity and therefore fails to provide close bone-to-implant contact, probably resulting in implant loosening and failure [23]. Accordingly, to obtain multifunctional implants for optimal clinical application, it is imperative to boost the osteogenic and anti-inflammatory activity together with fighting off bacterial contamination.

Currently, composite preparation and surface modification are two major strategies to improve the bioactivity of inert PEEK [24]. Some filler materials, such as hydroxyapatite, bioglass, calcium silicate, and silver particles are commonly used to prepare PEEK composites; besides, Pezzotti et al. incorporated  $\text{Si}_3\text{N}_4$  particles into a PEEK matrix to produce antibacterial, osteoconductive, and radiolucent spinal implants [24,25]. The surface determines the final capacity of an implant to integrate with surrounding tissue [2,26]. Aiming at realizing optimal osseointegration after implantation, PEEK surface modification is another preferred choice to improve its bioactivity without diminishing its numerous advantages. The most popular approach is to functionalize PEEK via bioactive coatings produced by physical or chemical methods. Many types of coatings, including calcium phosphate, biomolecules, hydroxyapatite, and titanium have been explored to enhance the osseointegration of PEEK implants [27–29]. Nevertheless, there remain multiple concerns, including degradation of the coatings, the need for complex and time-consuming chemical steps, and low bonding strength between the coatings and substrates. Surface modifications have focused on multifunctional properties such as improving biological activity, modulating inflammation, and avoiding bacterial infection, which are essential functions for physiologic osseointegration [30]. Although some research has been conducted on the combination of bacteriostasis and osseointegration [31–33], few studies have been reported concerning functionalizing the PEEK surface to obtain the key three properties of bacteriostasis, anti-inflammation, and osseointegration.

As a facile surface modification method, coating with adhesive polydopamine (pDA) is of particular interest [34]. By simple immersion, a structurally stable pDA film can be formed on many materials without any need for surface pretreatment [35]. The pDA-mediated surface modification coupled with bioactive molecules supporting bacteriostasis or osseointegration has been used to functionalize various biomaterials [36,37]. However, pDA cannot directly immobilize bioactive molecules within the cells, e.g., minocycline (Mino), a broad-spectrum tetracycline antibiotic and dexamethasone (Dex), a glucocorticoid noted for its anti-inflammation property and facilitation of osteogenesis [38,39]. Strategies to surmount this restriction include using nanomedicine formulations, such as liposomes, to carry, deliver, and slowly release these bioactive molecules into the cytoplasm [40].

Our previous research demonstrated that the mussel-inspired pDA coating of polystyrene (PS) surfaces, along with liposomes loaded with Mino and Dex, effectively mitigated the cell inflammatory response and prevented bacterial contamination *in vitro* [41]. However, the

osteogenic activity of Dex releasing from the functionalized PS surface has not been studied. Additionally, PS is not commonly used for orthopedic/dental implants. This multifunctional surface modification method has been further applied to improve bioinert PEEK, which is an extension of our earlier research. Herein, we evaluate the *in vitro* osteogenic activity of Dex/Mino liposome-modified PEEK and examine whether such a novel hard-tissue substitute could prevent bacterial contamination, attenuate foreign body response, and enhance osteogenesis for physiologic osseointegration *in vivo*. To the best of our knowledge, concurrent improvement of the PEEK surface for bacteriostasis, anti-inflammation, and osseointegration has great potential for clinical application; we herein demonstrate such improvements.

## 2. Experimental section

### 2.1. Preparation of Dex/Mino liposome-modified PEEK surfaces

Pristine PEEK was cut into different-sized disks. Those of dimensions  $\text{Ø}15 \times 2$  mm were used for the surface characterization and *in vitro* biological assay, while those  $\text{Ø}10 \times 1$  mm were used for *in vivo* subcutaneous implantation assay. For the *in vivo* beagle femur implantation model, cylindrical implants of dimensions  $\text{Ø}4 \times 7$  mm were prepared. Prior to use, the samples were polished with abrasive papers (400, 1000, 1500, and 2000 grit), ultrasonically cleaned for 2 h in acetone, anhydrous ethanol and deionized water sequentially, and dried at  $60^\circ\text{C}$ . Additionally, blank liposomes, Dex/Mino liposomes, and fluorescently labeled liposomes were prepared according to a thin-film hydration method [41].

The functionalized PEEK surfaces were prepared as previously described [41]. Briefly, dopamine hydrochloride (Sigma–Aldrich, USA) was first added to Tris-HCl solution (10 mM, pH 8.5; Aladdin, China) at a concentration of 2 mg/mL, and the pure PEEK samples were then immersed in the solution. The reaction was carried out under continuous shaking at 70 rpm for 18 h at  $37^\circ\text{C}$ . Thereafter, the resulting samples (named PEEK-pDA) were ultrasonically cleaned for 5 min followed by rinsing for three times and further immersed in blank liposome solution or Dex/Mino liposome solution for 24 h at  $37^\circ\text{C}$ . Then, the treated samples were gently washed for three times to remove physically adsorbed liposomes to provide two groups of samples (PEEK-blank lipo and PEEK-Dex/Mino lipo). The prepared PEEK disks were shown in Fig. S1.

### 2.2. Characterization

The water contact angle (WCA) of different PEEK surfaces was measured using a contact angle goniometer (SL200B; Kono, USA). Confocal laser scanning microscopy (CLSM; Carl Zeiss, Germany) was used to confirm the binding of fluorescently labeled liposomes onto the PEEK substrate, and a microplate reader (Elx808; BioTek, USA) was used to semiquantitatively measure the average fluorescence intensity of fluorescently labeled liposome-decorated PEEK surfaces. Prior to semiquantitative measurement, 400  $\mu\text{L}$  of methanol was used to dissolve the liposomes grafted on the PEEK substrates; then the fluorescently dissolved liquid was collected and measured. X-ray photoelectron spectroscopy (XPS; AXIS Ultra; Kratos Analytical, UK) was used to detect the surface chemical constituents and to confirm the presence of lipid films on liposome-modified surfaces. To explore the stability of the pDA coating (PEEK-pDA group) and the Dex/Mino liposome-modified coating (PEEK-Dex/Mino lipo group), all the prepared samples were immersed in 2 mL phosphate-buffered saline (PBS) at  $37^\circ\text{C}$  and were measured by XPS at preset times. Field emission scanning electron microscopy (FE-SEM; S-4800; Hitachi, Japan) was used to study the surface morphology of different PEEK samples. All samples were vacuum-dried and sprayed with gold before observation. The surface roughness of different PEEK samples was characterized by an atomic force microscopy (AFM, PI3800/SPA400, Seiko Instruments, Japan).

The scan range was  $10\ \mu\text{m} \times 10\ \mu\text{m}$ .

### 2.3. *In vitro* cytocompatibility evaluation

#### 2.3.1. Cell culture

Human mesenchymal stem cells (hMSCs; ATCC, USA) were cultured in normal growth medium containing Dulbecco's modified Eagle's medium (DMEM; HyClone, USA), 10% fetal bovine serum (Gibco; Thermo Fisher Scientific, USA), and 1% penicillin/streptomycin (Gibco). The cells were used between passages four to eight. The cells were seeded on different PEEK samples in 24-well plates at a density of  $3 \times 10^4$  cells per well. The culture medium was changed every 2 days.

#### 2.3.2. Cytoskeletal observations

After 1 and 3 days of culture, cells on different PEEK surfaces were fixed with paraformaldehyde (4% v/v) for 20 min, permeabilized with Triton X-100 (0.1% v/v) for 5 min, and dyed with  $5\ \mu\text{g}/\text{mL}$  FITC-phalloidin (Sigma) for 30 min. Then, the cells were stained with  $10\ \mu\text{g}/\text{mL}$  of 4',6-diamidino-2-phenylindole (DAPI; Roche, Germany) for 5 min and imaged using CLSM.

#### 2.3.3. Cell morphology imaging using scanning electron microscopy

After 1 and 3 days of culture, cells on different PEEK surfaces were fixed with glutaraldehyde (2.5% v/v) for 2 h and dehydrated in gradient ethanol (30, 50, 60, 70, 80, 90, and 100%) for 15 min. Then, the samples were vacuum-dried, sprayed with gold, and observed by SEM.

#### 2.3.4. Cell proliferation assay

The cell proliferation on different PEEK samples was assayed using a cell counting kit (CCK-8; Dojindo, Japan) per the manufacturer's instructions. Briefly, at 1, 3, 5, and 7 days, the culture medium was aspirated and CCK-8 reagent was added to each well with new culture medium at 1:10 v/v, away from light. After 2 h of incubation at  $37\ ^\circ\text{C}$ , the supernatant (100  $\mu\text{L}$ ) from each well was added to a 96-well plate, and the optical density (OD) was measured using a plate reader.

#### 2.3.5. Live/dead assay

A live/dead staining kit (Dojindo) was used to evaluate the viability of hMSCs on different PEEK samples per the manufacturer's instructions. At day 4, the samples were stained with  $2\ \mu\text{M}$  calcein-AM (live cells, green fluorescence) and  $4.5\ \mu\text{M}$  PI (dead cells, red fluorescence) for 5 min at  $37\ ^\circ\text{C}$  away from light. Images were captured by CLSM.

### 2.4. Osteogenic bioactivity evaluation of liposome-functionalized surfaces

hMSCs were seeded on six-well PS culture plates at a density of  $1 \times 10^5$  cells per well. After 48 h of incubation, the normal growth medium was removed and replaced with Dex-existent osteogenic differentiation medium containing Dex (100 nM; Sigma), ascorbic acid (50  $\mu\text{g}/\text{mL}$ ; Sigma), and  $\beta$ -glycerophosphate (10 mM; Sigma) or Dex-absent osteogenic differentiation medium containing ascorbic acid (50  $\mu\text{g}/\text{mL}$ ; Sigma) and  $\beta$ -glycerophosphate (10 mM; Sigma). The Dex-existent osteogenic differentiation medium (also called the osteoinductive medium) and Dex-absent osteogenic differentiation medium (also called the osteoconductive medium) were labeled as + and -, respectively. The medium was changed every 2 days. According to the presence or absence of Dex in the osteogenic differentiation medium and the different modification of PS surfaces, the experiment was divided into four groups: blank lipo (-) group, blank lipo (+) group, Dex/Mino lipo (-) group, and Dex/Mino lipo (+) group.

#### 2.4.1. Alkaline phosphate activity quantification and staining

An alkaline phosphate (ALP) activity assay kit (Nanjing Jiancheng Biotechnology, China) was used to quantify the ALP activity of hMSCs on different samples. Briefly, hMSCs were first scraped from the

surfaces using Triton X-100 (1% v/v) after 3 and 7 days of cultivation. Then the cell-lysis solution was collected and centrifuged (12,000 rpm at  $4\ ^\circ\text{C}$ ) for 30 min to remove all cell debris. Then, supernatant (30  $\mu\text{L}$ ) was mixed with the ALP assay working solution and measured at 520 nm using a plate reader. For standardization, a bicinchoninic acid (BCA) protein assay kit (Thermo Fisher Scientific) was used to determine the total protein concentration. The ALP activity value was standardized and expressed as the total protein content (U/gprot). For ALP staining, the hMSCs on a liposome-decorated surface were first fixed by 95% cold ethanol for 30 min. Staining was then performed using a BCIP/NBT ALP color development kit (Beyotime Biotechnology, China) for 30 min per the manufacturer's instructions.

#### 2.4.2. Alizarin Red S staining and quantification

Alizarin Red S (ARS) staining was used to evaluate mineralized nodule formation on day 21. Briefly, hMSCs on different samples were fixed in 4% paraformaldehyde for 30 min. Then, ARS solution (2%, pH 4.2; Sigma-Aldrich) was added and the sample incubated for 20 min. Excess ARS was thoroughly removed with deionized water and the deposited calcium was imaged using a microscope. For quantification, the stained samples were immersed in hexadecylpyridinium chloride (1 w/v%; Sigma-Aldrich) for 2 h with shaking, followed by detection at 550 nm using a plate reader.

#### 2.4.3. Real-time polymerase chain reaction

At day 14, total mRNA of hMSCs was isolated using TRIzol (Invitrogen, USA) and reverse-transcribed into cDNA using a RevertAid First Strand cDNA Synthesis Kit (Thermo Fisher, USA) per the manufacturer's instruction. Then, real-time polymerase chain reaction (RT-PCR) was carried out using an ABI 7500 RT-PCR instrument (Applied Biosystems, USA) with SYBR Green dye (Roche). The primers (5'-3') employed in this study are listed in Table S1;  $\beta$ -actin was used as a housekeeping gene. Cycle threshold (Ct) values were used to determine fold differences according to the  $\Delta\Delta\text{Ct}$  method.

#### 2.4.4. Immunofluorescence

At day 21, hMSCs on different samples were fixed with paraformaldehyde (4%) for 30 min, permeabilized with Triton X-100 (0.2% v/v) for 30 min, and incubated with 3% bovine serum albumin solution (Sigma-Aldrich) for 2 h at  $37\ ^\circ\text{C}$  to block nonspecific binding. Cells were then incubated overnight at  $4\ ^\circ\text{C}$  with primary antibodies: mouse monoclonal antihuman runt-related transcription factor 2 (Runx2; 1:200; Abcam, UK), rabbit monoclonal antihuman osteopontin (OPN; 1:200; Abcam), mouse monoclonal antihuman osteocalcin (OCN; 1:200, Abcam), and rabbit polyclonal antihuman type I collagen alpha 1 (Col1 $\alpha$ 1; 1:200; Abcam). Next, cells were incubated with secondary antibodies (fluorescein-conjugated goat anti-mouse IgG and rhodamine (TRITC)-conjugated goat anti-rabbit IgG) at a dilution of 1:200 for 1 h away from light. DAPI (1  $\mu\text{g}/\text{mL}$ ; Sigma-Aldrich) was used to stain cell nuclei for 5 min. All staining steps were followed by three washes in PBS. Finally, cells were imaged by CLSM.

### 2.5. Osteogenic bioactivity evaluation of Dex/Mino liposome-modified PEEK surfaces

hMSCs were seeded at a density of  $3 \times 10^4$  cells per well in bare PEEK and Dex/Mino liposome-coated PEEK. After 48 h of incubation, the normal growth medium was removed and replaced with osteoinductive medium (containing 100 nM Dex, 10 mM  $\beta$ -glycerophosphate, and 50  $\mu\text{g}/\text{mL}$  ascorbic acid) or osteoconductive medium (containing 10 mM  $\beta$ -glycerophosphate and 50  $\mu\text{g}/\text{mL}$  ascorbic acid). In this section, we used the + and - symbols on behalf of osteoinductive medium (also called the Dex-existent osteogenic differentiation medium) and osteoconductive medium (also called the Dex-absent osteogenic differentiation medium), respectively. The medium was changed every 2 days. According to the osteoinductive or

osteoconductive medium and the different modification of PEEK surfaces, the experiment was divided into four groups: PEEK (–) group, PEEK-Dex/Mino lipo (–) group, PEEK (+) group, and PEEK-Dex/Mino lipo (+) group. ALP and ARS studies were conducted as described in Sections 2.4.1 and 2.4.2, respectively.

## 2.6. *In vitro* and *in vivo* bacteriostasis assays

### 2.6.1. Bacterial cultures

The bacteriostatic effect on Gram-positive *Streptococcus mutans* (*S. mutans*; UA159; ATCC) and Gram-negative *Porphyromonas gingivalis* (*P. gingivalis*; W83; ATCC) was evaluated. *S. mutans* were cultured in Todd-Hewitt broth (TH) medium. *P. gingivalis* were cultured in brain heart infusion (BHI; Oxoid, Canada) and agar with 5 µg/mL hemin, 5 mg/mL yeast extract, 1 µg/mL vitamin K1, 1 mg/mL L-cysteine, and 1:20 (v/v) defibrinated sheep blood. All samples of *S. mutans* were cultured in an incubator (containing 5% CO<sub>2</sub>) for the scheduled times at 37 °C. All samples of *P. gingivalis* were grown in an anaerobic bag (Thermo Fisher) for the scheduled times at 37 °C.

### 2.6.2. Quantitative measurement of bacterial adhesion and proliferation

The Microbial Viability Assay Kit-WST (Dojindo) was used to assess the antibacterial activity of bare PEEK and Dex/Mino liposome-modified PEEK. At the scheduled times, PEEK samples were removed, lightly cleaned, and placed into fresh 24-well plates. Thereafter, WST reagent with culture medium at a ratio of 1:20 (v/v) was added to each well. The incubation was done for 2 h at 37 °C away from light. Then, 100 µL of supernatant was transferred to a 96-well plate followed by measurement of the OD at 450 nm using a plate reader.

### 2.6.3. Live/dead fluorescent staining

The antibacterial effect of different PEEK samples was further investigated by a LIVE/DEAD BacLight Bacterial Viability Kit (L-7007; Invitrogen). Briefly, incubated samples were stained with a 1:1 mixture of SYTO 9 (live bacteria, green fluorescence) and PI (dead bacteria, red fluorescence) for 15 min away from light, washed lightly with PBS, and observed using CLSM.

### 2.6.4. *In vivo* antibacterial study

All surgical experiments were approved by our Animal Ethics Committee (Approval No.: 123456). Seven C57BL/6 mice (7 weeks, male) were used in this study. The Dex/Mino liposome-modified PEEK and bare PEEK (control) were subcutaneously implanted into C57BL/6 mice to evaluate the *in vivo* bacteriostatic action of different PEEK surfaces and their histological influence. Before operating, each C57BL/6 mouse was anesthetized with 1% pentobarbital sodium via an intraperitoneal injection. Next, we shaved the dorsal of each mouse followed by sterilizing using povidone iodine. Successively, we created a longitudinal incision, bluntly dissected a subcutaneous pocket, placed the PEEK disks (one disk per mouse, Ø10 × 1 mm) and seeded 10 µL of *S. mutans* ( $1 \times 10^8$  CFU mL<sup>-1</sup>) onto the PEEK surfaces before closing the incision with surgical suture.

The mice were euthanized 24 h after implantation, and the implants were gently removed. For bacterial quantification, the tissue fluids were diluted and spread onto agar plates. The numbers of colonies were counted after incubating for 2 days.

### 2.7. *In vivo* anti-inflammation study

For the subcutaneous implant-associated inflammatory reaction model, we didn't seed bacteria on different PEEK surfaces; except for this difference, the surgical procedure was the same as in Section 2.6.4. Fourteen C57BL/6 mice (7 weeks, male) were used in this section. After implantation, the mice were euthanized at day 1. The samples from each group were collected, and the subcutaneous tissues separated from the implants were fixed in 4% paraformaldehyde, followed by paraffin

embedding and sectioning for further hematoxylin and eosin (HE) staining evaluation. The samples harvested at day 1 were also collected for further enzyme-linked immunosorbent assay (ELISA) testing. The subcutaneous tissues were separated from the implants and immersed into physiological saline followed by homogenizing with a beater. The tissue homogenate was then centrifuged at 3000 rpm for 10 min. The supernatant was collected and further used for the quantification of tumor necrosis factor-α (TNF-α) and interleukin-6 (IL-6) using mouse ELISA kits per the manufacturer's protocol.

## 2.8. *In vivo* new bone formation study

### 2.8.1. Surgical implantation

The procedures were approved by the Animal Ethics Committee (Approval No.: 789012). Sixteen PEEK implants (Ø4 × 7 mm with screw threads) were randomly assigned to the two groups (PEEK-Dex/Mino lipo and PEEK control). General anesthesia was performed on three male beagle dogs (1.5 years, 11.2 ± 0.6 kg) using an intravenous injection of 3% pentobarbital sodium (1 mL/kg). The samples were implanted into the prepared holes (Ø4 × 7 mm using a dental drill) on each side of the femur. For each femur, two or three cylindrical implants were placed randomly. The dogs received intramuscular injection of penicillin sodium (10 U/kg) for 3 days after surgery and were euthanized at 8 weeks. The bone samples with implants were fixed in 10% neutral formalin (Solarbio, China) for further analysis.

### 2.8.2. Micro computed tomography and histological analyses

Micro computed tomography (micro-CT; Inveon MM CT; Siemens Medical Solutions, USA) was used to scan the harvested femurs, and Inveon Research Workplace software (Siemens) was used to reconstruct the two-dimensional (2D) and three-dimensional (3D) models and quantify the newly formed bone mass. After, the undecalcified femurs were dehydrated with an ascending ethanol gradient, embedded in methyl methacrylate resin, and sectioned with a microtome (SP1600; Leica, Germany). HE staining and toluidine blue staining were performed to examine the new bone growth.

## 2.9. Statistical analysis

Origin 8.0 software (OriginLab, USA) was used for the statistical analyses. Data are expressed as means ± standard deviation. A one-way analysis of variance and the Tukey *post hoc* test were used to identify statistically significant differences (p) among groups; p values < 0.05 indicated statistical significance.

## 3. Results and discussion

### 3.1. Development and characterization of Dex/Mino liposome-decorated PEEK surfaces

Fig. S2 shows the preparation of Dex/Mino liposome-decorated pDA-coated PEEK and its bacteriostasis and anti-inflammatory and osseointegrative properties, *in vitro* and *in vivo*, for load-bearing bone repair. In the present work, inert PEEK was first covered by pDA due to its strong adhesion, and then the Dex/Mino liposomes were coated onto the pDA layer via the covalent linkage between catechol moieties from pDA and amine groups of the liposomes. After these two surface treatment steps, kinds of characterization methods were used to detect any changes in the prepared Dex/Mino liposome-decorated PEEK surfaces.

The WCA was used to explore the wettability of the sample surfaces (Fig. 1a). The WCA of bare PEEK was 71°, whereas that of pDA-coated PEEK was much lower (24°) due to successful modification with hydrophilic dopamine molecules. Conversely, the WCAs of the liposome-decorated PEEK groups increased to approximately 61°. This change in wettability indicated the successful modification with hydrophobic

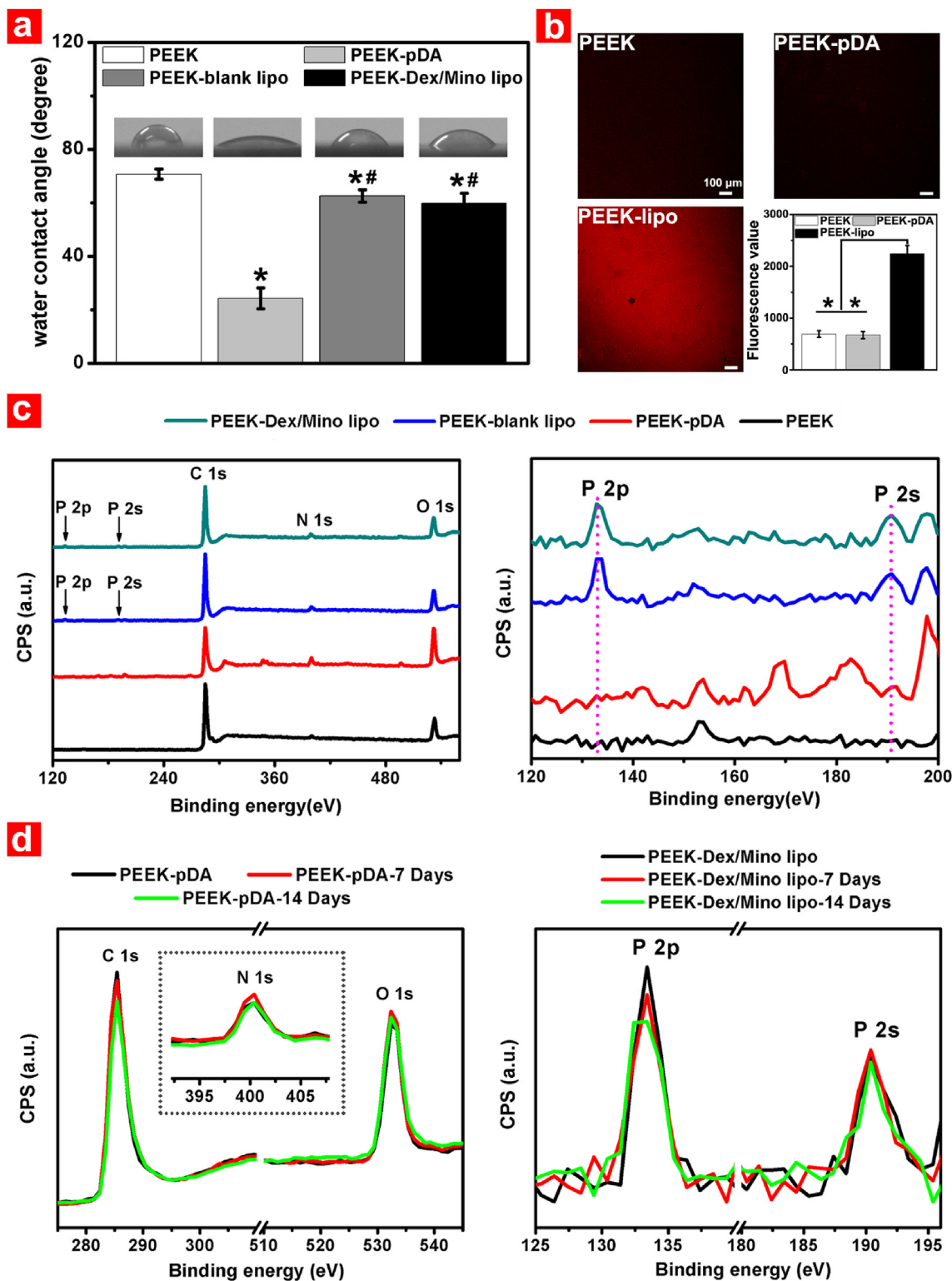


**Fig. 1.** Surface characterization of different PEEK samples. (a) Water contact angle measurements. \*, #:  $p < 0.05$  compared with PEEK and PEEK-pDA group, respectively. All data represent the mean  $\pm$  SD ( $n = 6$ ). (b) Fluorescently labeled liposomes immobilized onto PEEK substrates and their semiquantitative grafted-liposome intensity. \*: Significant difference between the PEEK-lipo group and PEEK or PEEK-pDA group ( $p < 0.05$ ). All data represent the mean  $\pm$  SD ( $n = 6$ ). (c) X-ray photoelectron survey scan spectra of different PEEK samples. (d) X-ray photoelectron survey scan spectra of PEEK-pDA (C 1s, N 1s and O 1s) and PEEK-Dex/Mino lipo (P 2p and P 2s) before and after immersion in phosphate-buffered saline for 7 and 14 days.

liposomes of the pDA-coated PEEK surfaces. The WCAs of the liposome-coated PEEK groups were about  $10^\circ$  lower than those of their pristine PEEK counterparts, indicating slightly improved hydrophilicity of the functionalized PEEK surfaces.

Fluorescently labeled liposomes were used to reveal the spatial distribution of liposomes grafted on the surface of pDA-coated PEEK samples. Fig. 1b shows typical fluorescence images and their matching semiquantitative grafted-liposome intensities. The PEEK or PEEK-pDA

samples prepared without modification and immersion in fluorescently labeled liposomes showed no red fluorescence signal, illustrating no autofluorescence and no covalent attachment of the liposomes on the PEEK surfaces. In contrast, the red fluorescent liposomes were uniformly dispersed on the surface of the functionalized PEEK (PEEK-lipo group). The semiquantitative fluorescence values further confirmed successful liposome modification. In addition, we also measured the fluorescence intensity of the liposome-attached PEEK samples prepared without pDA coating (named as PEEK-NF-lipo; NF: non functionalized). Fig. S3 shows that the fluorescently labeled liposomes attached to both PEEK-NF-lipo and PEEK-lipo substrates; the red fluorescence intensity of PEEK-lipo group was stronger than that of PEEK-NF-lipo group, which was consistent with the semiquantitative results. Accordingly, we speculated that much more fluorescently labeled liposomes might be immobilized onto the PEEK surface due to the presence of pDA coating.

Fig. 1c and Table S2 illustrate the surface chemistry composition of different PEEK samples determined by XPS. Prominent C 1s and O 1s peaks were observed for the PEEK sample. After grafting the pDA on the PEEK surface (PEEK-pDA group), the contents of N 1s and O 1s increased from 1.25% to 5.73% and 11.86–20.85%, respectively; while the relative content of C 1s decreased to 73.41% from 86.89%. The changes in element contents were attributed to the successful anchoring of pDA coating which contained numerous amino ( $-NH_2$ ) and hydroxyl ( $-OH$ ). In PEEK-blank lipo and PEEK-Dex/Mino lipo groups, a small phosphorus (P 2p and P 2s) peak appeared and the corresponding content of P 2p increased to 0.79% and 0.93%, respectively. This was consistent with surface modification of the lipid films on PEEK.

As is well-known, the key to assure the security of implanted devices *in vivo* is the good stability [42]. Hence, XPS was further used to test the static stability of the pDA coating (PEEK-pDA group) and the Dex/Mino liposome-functionalized coating (PEEK-Dex/Mino lipo group) at preset times. As shown in Fig. 1d, little change was found in scan spectra of PEEK-pDA (C 1s, N 1s and O 1s) before and after immersion in PBS for 7 and 14 days; this result indicated that pDA coating had good stability, which was consistent with the result previously reported by Zhang et al. [42]. In PEEK-Dex/Mino lipo group, the spectra area of P 2p mildly decreased after immersion in PBS for 7 and 14 days and the spectra area of P 2s remained almost constant until the 14 days of the study. This result indicated that the Dex/Mino liposome-functionalized coating had acceptable stability. In addition, we also explored the stability of the Dex/Mino liposome-attached coating prepared without pDA coating (named as PEEK-NF-Dex/Mino lipo group; NF: non functionalized). By contrast, the spectra area of P 2p in the PEEK-NF-Dex/Mino lipo group sharply decreased and the spectra area of P 2s was hardly detected after immersion for 7 and 14 days in PBS (Fig. S4). The sharp contrast between the functionalized and non-functionalized coatings was also in accordance with the result previously reported by López-Noriega et al. [43]. Fig. S5 compared the scan spectra of PEEK-NF-Dex/Mino lipo and PEEK-Dex/Mino lipo groups before (a) and after immersion in PBS for 7 (b) and 14 (c) days. It was obvious that the spectra areas of P 2p and P 2s in PEEK-Dex/Mino lipo group were larger than that of the PEEK-NF-Dex/Mino lipo group at preset times. Hence, the covalently grafted coating (PEEK-Dex/Mino lipo group) might hold higher binding between the lipids layer and the substrate, and present more stability than the non-functionalized coating (PEEK-NF-Dex/Mino lipo group). In addition, these results also confirmed that pDA coating was required for liposome modification on PEEK surfaces in the current study.

Fig. 2a and b shows SEM and AFM images that illustrate the surface morphology and surface roughness of different PEEK samples. The bare PEEK sample had a smooth surface morphology ( $R_a = 22.25 \pm 3.62$  nm), while a rough surface morphology ( $R_a = 53.53 \pm 4.42$  nm) with numerous pDA particles was found for the PEEK-pDA group, consistent with pDA surface modification. In addition, the immobilization of Dex/Mino liposomes on the PEEK-pDA surface (PEEK-Dex/Mino lipo group) somewhat decreased the surface roughness

( $R_a = 35.90 \pm 4.86$  nm), consistent with the presence of the liposome layer. The inset image (Fig. 2a) shows an immobilized liposome about 150 nm. In addition, Fig. S6 shows the AFM image that illustrates the surface morphology and surface roughness ( $R_a = 41.80 \pm 3.90$  nm) of the PEEK-NF-Dex/Mino lipo group. Several scattered nano-objects ( $\sim 400$  nm) and an irregular micro-object ( $\sim 3.5 \mu\text{m}$ ) composed of many round-shaped nano-objects (about 150–250 nm) were found. The formation of large aggregate was probably due to the agglomeration effect. By contrast, we found that the round-shaped nano-objects (about 100–200 nm) homogeneously dispersed on the surface of PEEK-Dex/Mino lipo group (Fig. 2b). Accordingly, we speculated that the formation of covalent linkage between catechol moieties from pDA and amine groups of the liposomes might play an important role in reducing the agglomeration effect.

Taken together, we concluded that Dex/Mino liposomes were stably decorated on the pDA-coated PEEK surfaces.

### 3.2. Cytocompatibility evaluation of Dex/Mino liposome-decorated PEEK surfaces

Cell adhesion is closely related to cellular functions and *in vivo* tissue reconstruction, and cell proliferation is fundamental to producing the bone mineralized matrix [44]. Significant bone tissue can be produced around implants via cell adhesion and proliferation [44]. Therefore, cell adhesion and proliferation of hMSCs on the Dex/Mino liposome-decorated PEEK surfaces are key elements that must be investigated for any application (such as orthopedic/dental implants) of this material in biomedical fields.

To investigate the interaction between cells and samples, the cytoskeleton (F-actin) of hMSCs grown on different PEEK surfaces was imaged using CLSM after 1 and 3 days. At day 1 (Fig. S7a), the hMSCs exhibited narrow spreading and a filamentous morphology on the modified PEEK surfaces, and F-actin was poorly developed. More cells attached to the pure PEEK surfaces, while a few cells attached to the modified PEEK surfaces. After 3 days of incubation (Fig. 3a), obvious cytoplasmic actin skeletons and distinct cell-cell contacts were evident on all samples. The cells spread adherent filopodia and extended mature F-actin intracellular stress fibers. Likewise, cells grown on all samples proliferated to completely cover the surfaces. The adhesion morphologies of hMSCs incubated on as-prepared sample surfaces after 1 and 3 days were further assessed by SEM. After 1 day of culture (Fig. S7b), the attached cells on all samples started to spread, displaying a polygonal shape with extended lamellipodia. The bare PEEK group had more cells attached than the PEEK-Dex/Mino lipo one, and the PEEK-Dex/Mino lipo group had more cells attached than the PEEK-blank lipo one. After 3 days of culture (Fig. 3b), cells with filopodia were tightly attached to the surfaces of both the bare PEEK and modified PEEK samples. Moreover, cells agglomerated and occupied nearly the entire substrate surface, which was consistent with the CLSM results. Thus, the SEM and fluorescence images implied that the liposome-decorated surfaces had good cytocompatibility and could also facilitate normal adhesion morphology of hMSCs.

Desirable implant surfaces assist cell adhesion and facilitate cell proliferation. The CCK-8 assay results (Fig. 3c) show that the hMSCs on all PEEK samples proliferated in a time-dependent manner during the culture period. The increasing OD values indicated that the liposome-modified PEEK surfaces promoted cell growth with increasing time (1, 3, 5, and 7 days). Nonetheless, the OD values obtained for the liposome-decorated PEEK groups were slightly lower than those obtained for the pristine PEEK control group ( $p < 0.05$ ), suggesting that the liposome-decorated PEEK surfaces had a slightly negative effect on cytocompatibility. This difference might be attributed to the PEGylated coating of lipids and the non-specific serum-protein absorption [45]. Although the liposomes served as carriers for Dex and Mino and may have partly lowered initial cell adhesion, subsequent cell proliferation was not affected. We thus inferred that the liposome-decorated PEEK surfaces had

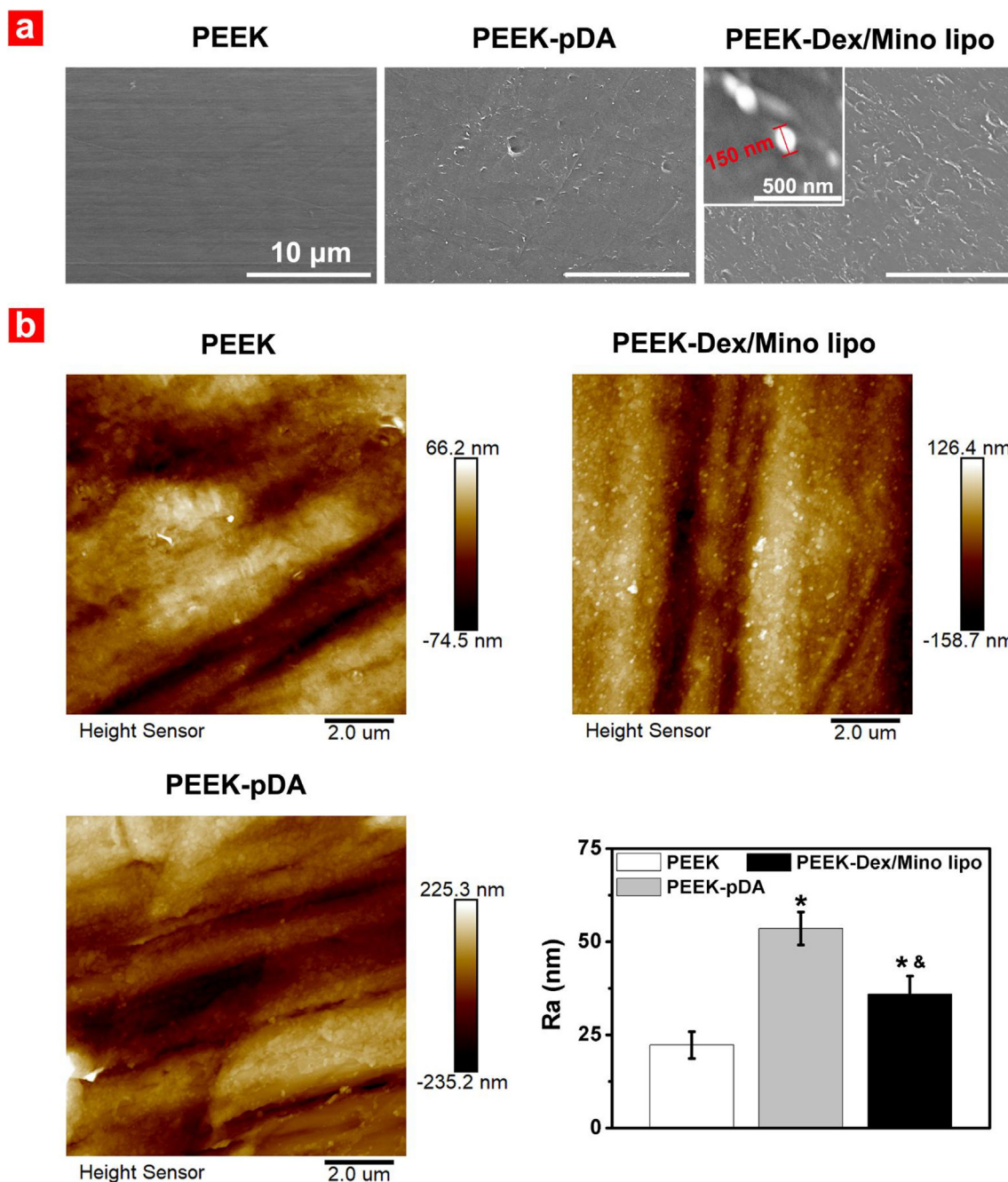


**Fig. 2.** The surface morphology and surface roughness of different PEEK samples. (a) Scanning electron microscopy images. (b) Atomic force microscopy images and the surface roughness of PEEK, PEEK-pDA, and PEEK-Dex/Mino lipo samples. \*, &:  $p < 0.05$  compared with PEEK and PEEK-pDA, respectively. All data represent the mean  $\pm$  SD ( $n = 4$ ).

acceptable cytocompatibility. Additionally, the PEEK-Dex/Mino lipo group showed higher OD values than the PEEK-blank lipo group during all cultivation periods, hinting that suitable surface modification with Dex and Mino provided the surfaces with much more favorable cytocompatibility despite a somewhat negative influence of liposome modification. Calcein-AM/PI staining revealed that the hMSCs grew well on all PEEK groups and the ratio of dead cells in each group was very low after 4 days of incubation, suggesting that both pure and modified PEEK possessed good cytocompatibility toward hMSCs (Fig. 3d). Overall, on the basis of cell adhesion, proliferation, and vitality studies, we concluded that Dex/Mino liposome-decorated PEEK surfaces displayed acceptable cytocompatibility and might be suitable for orthopedic/dental implants.

### 3.3. Osteogenic differentiation of hMSCs cultured on liposome-functionalized surfaces

The optimal biointerface to enhance implant osseointegration displays favorable cytocompatibility and effective osteogenic activity. For the convenience of experimental operation and observation, we first used PS culture plates as the basal surfaces to evaluate whether Dex released from the Dex/Mino liposome-decorated surfaces was efficient at enhancing the osteogenic differentiation of hMSCs. Measurement of the ALP activity, calcium deposition amount, gene expression, and corresponding marker protein expression levels were made to explore the osteogenesis capacity of hMSCs on the Dex/Mino liposome-modified PS surface. The + and - symbols refer to Dex-existent osteogenic

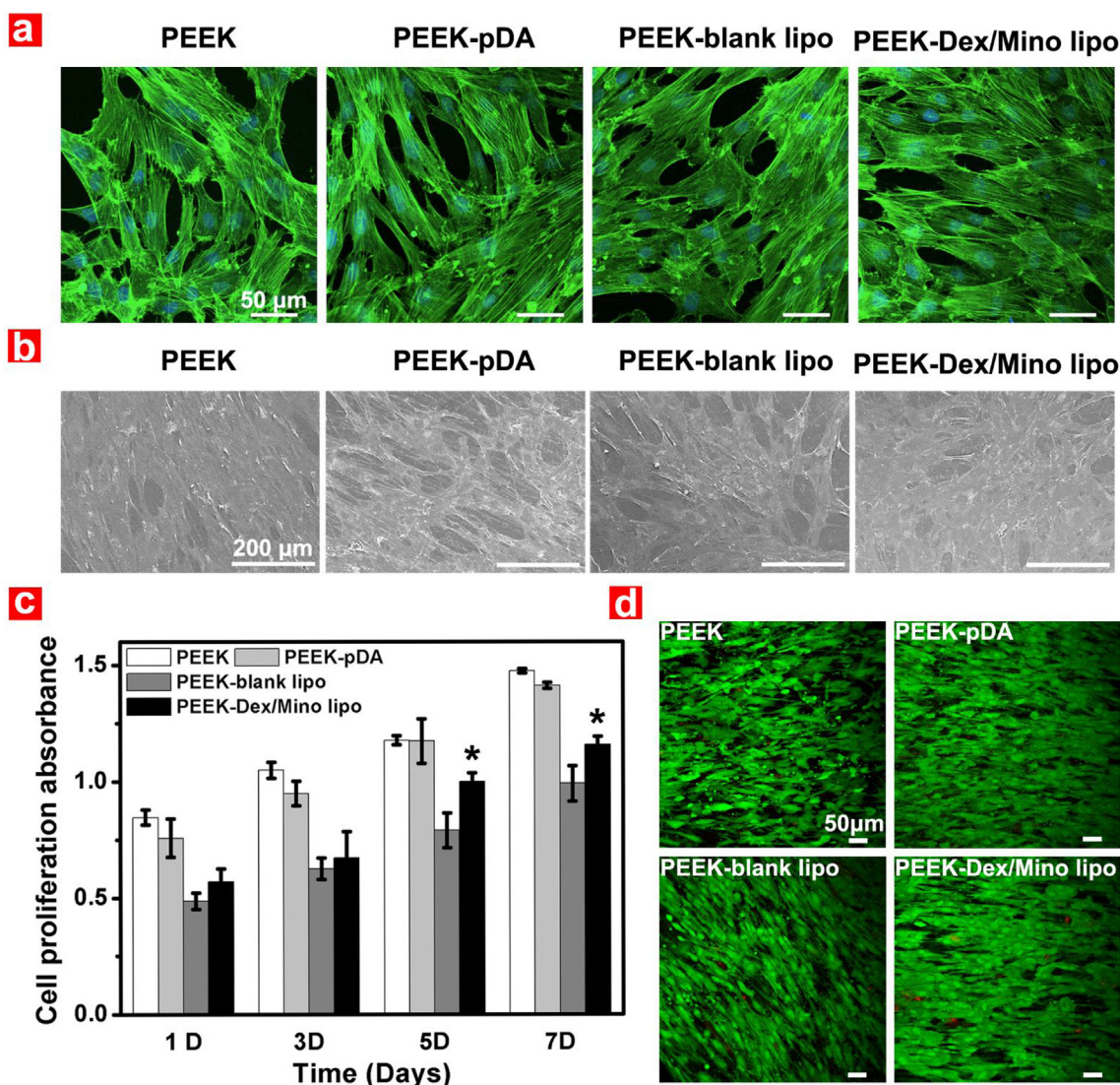


**Fig. 3.** Adhesion, proliferation, and viability of hMSCs on different PEEK surfaces. (a) Confocal laser scanning microscopy and (b) Scanning electron microscopy observations of adhering hMSCs cultured on different PEEK surfaces for 3 days (green, labeled with FITC-phalloidin, counterstained with DAPI to show nuclei in blue). (c) Proliferation of hMSCs cultured on different PEEK surfaces. \*: Significant difference between the PEEK-blank lipo and the PEEK-Dex/Mino lipo groups ( $p < 0.05$ ). All data represent the mean  $\pm$  SD ( $n = 6$ ). (d) Viability of hMSCs cultured for 4 days on different PEEK surfaces labeled by calcein-AM/PI staining. Live cells: green; dead cells: red.

differentiation medium (also called the osteoinductive medium) and Dex-absent osteogenic differentiation medium (also called the osteoconductive medium), respectively.

### 3.3.1. Alkaline phosphatase activity and matrix mineralization

Alkaline phosphatase is a pivotal indicator of osteogenic differentiation; increasing ALP activity is a crucial event that happens in the early phase of osteogenesis [46]. Fig. 4a shows the ALP expression level of hMSCs cultured on different surfaces at preset times. As expected, the hMSCs cultured on the Dex/Mino lipo (–) group after 3 and 7 days expressed stronger ALP activity than the cells cultured on the blank lipo (–) group due to the presence of Dex (which is well-known for inducing osteogenic differentiation [47]) released from the Dex/Mino liposome-decorated surfaces. Similarly, the ALP activity of the Dex/Mino lipo (+) group was stronger than that of the blank lipo (+) group, indicating that the Dex/Mino liposome was successfully modified on the PS surface and the releasing Dex was active. Furthermore, at day 3, there was no statistically significant difference in ALP activity expression between the Dex/Mino lipo (–) and blank lipo (+) groups. This result indicates that the Dex releasing from the liposomes and

immobilized on the surface was at least as effective as Dex in the standard osteogenic culture medium. However, at day 7, a lower level of ALP expression was found for the Dex/Mino lipo (–) group than the blank lipo (+) group. We suggest that the amount of Dex released may have been insufficient to drive the osteogenic differentiation under this time point. Even so, the Dex/Mino lipo (+) group exhibited the highest up-regulation of ALP activity of hMSCs at that same time point due to the accumulative effect of Dex released from the surface modification and supplemented in the culture medium. The ALP staining (Fig. 4b) confirmed these findings and demonstrated that Dex/Mino liposome modification could enhance hMSCs osteogenesis.

Calcium deposition is another crucial marker of osteogenic differentiation, and the up-regulation of its expression is a critical event during the late-stage of osteogenesis [48]. At day 21, ARS staining and quantification were performed to assay the efficiency of the mineralization stage. Fig. 4c and d shows that both the Dex/Mino lipo (–) and Dex/Mino lipo (+) groups expressed higher amounts of mineralized matrix than the blank lipo (–) and blank lipo (+) groups, implying the osteogenic advantage of the Dex/Mino liposome-modified surface over the blank liposome-modified surface. Moreover, when

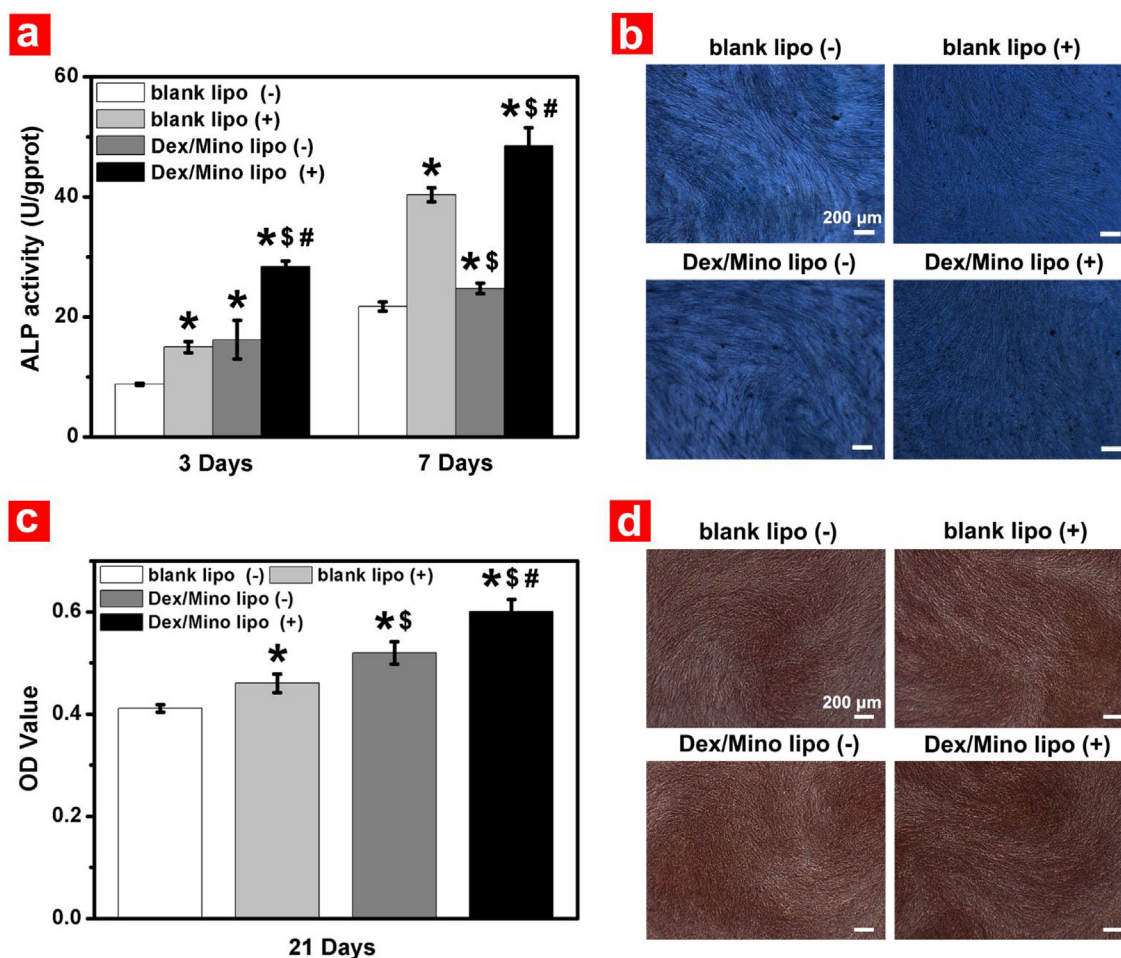


**Fig. 4.** Effect of liposome-modified polystyrene surfaces on ALP expression of hMSCs and calcium deposition. (a) Determination of ALP activity at 3 and 7 days and (b) representative staining of ALP on day 7. (c) Determination of calcium deposition on day 21 and (d) representative Alizarin Red S staining. \*, \$, #:  $p < 0.05$  compared with blank lipo (-), blank lipo (+), and Dex/Mino lipo (-), respectively. All data represent the mean  $\pm$  SD ( $n = 6$ ). The + and - symbols refer to Dex-existent osteogenic differentiation medium (also called the osteoinductive medium) and Dex-absent osteogenic differentiation medium (also called the osteoconductive medium), respectively.

comparing the Dex/Mino lipo (-) and blank lipo (+) groups, it was evident that despite not introducing Dex in the culture medium, the elevating influence of the functionalized surface on calcium deposition was still obvious; this was due to the introduction of Dex released from the Dex/Mino liposomes. Remarkably, Dex-treated hMSCs incubated on the Dex/Mino lipo (+) group exhibited the largest amount of calcium deposition, affirming that the Dex/Mino liposome modification induced osteogenesis by improving mineralization. Summarizing, the ALP and ARS assays illustrated that the Dex/Mino liposome-modified surfaces possessed excellent osteoinductive ability.

### 3.3.2. Osteo-related marker expression

Osteogenic gene expression and immunofluorescent staining analyses were used to further investigate the osteogenic differentiation ability of the functionalized surface. Fig. 5 shows the change in expression of osteogenic differentiation-related markers, including ALP (an early stage marker), OPN (a midstage marker), OCN (a late-stage marker), Runx2 (osteoblast-specific transcription factor), and Col1 $\alpha$ 1 (a marker related to production of extra cellular matrix) [49,50]. At day 14, all of the osteo-associated genes were up-regulated in the Dex/Mino lipo (-) group compared with the blank lipo (-) group. Additionally, the expression levels of OCN and Col1 $\alpha$ 1 were slightly higher for the Dex/Mino lipo (-) group than for the blank lipo (+) group. Notably, all of the gene expression levels in the Dex/Mino lipo (+) group were lower than those in other groups ( $p < 0.05$ ). Considering that the

effective concentration of Dex in the stimulatory process of osteogenic differentiation was only 100 nM, higher concentrations of Dex might exert inhibitory effects by down-regulating the gene expression receptors and further weakening the osteogenic response to Dex [51,52]. Accordingly, at this time stage, the reduced gene expression levels for the Dex/Mino lipo (+) group were influenced by the high concentrations of Dex accumulated by both release from the functionalized surfaces and addition to the culture medium. The osteo-related protein expression at 21 days was further explored to confirm the ALP, ARS, and gene analyses. Representative immunofluorescent staining images (Fig. 5b) revealed that hMSCs cultured on the Dex/Mino liposome-modified surface were characterized by improved production of osteogenic-associated proteins.

As a usual supplement in osteogenic medium, Dex is an effective stimulator to improve the *in vitro* osteogenic differentiation of MSCs [51]. The loading of Dex into liposomes might underlie its sustained delivery efficacy, extended stability, and bioactivity, thereby enhancing osteogenesis. By immobilizing the liposomes onto the PS surface, we gained the advantage of releasing the encapsulated Dex in the immediate vicinity of the cells, thereby boosting its bioavailability with no need to further supplement the Dex in the culture medium. The results above corroborated that immobilizing the Dex/Mino liposomes onto the surface where the hMSCs were attached was effective at improving osteogenic differentiation. This effect might be due to the direct interaction between Dex/Mino liposomes and cells, or even to the cells

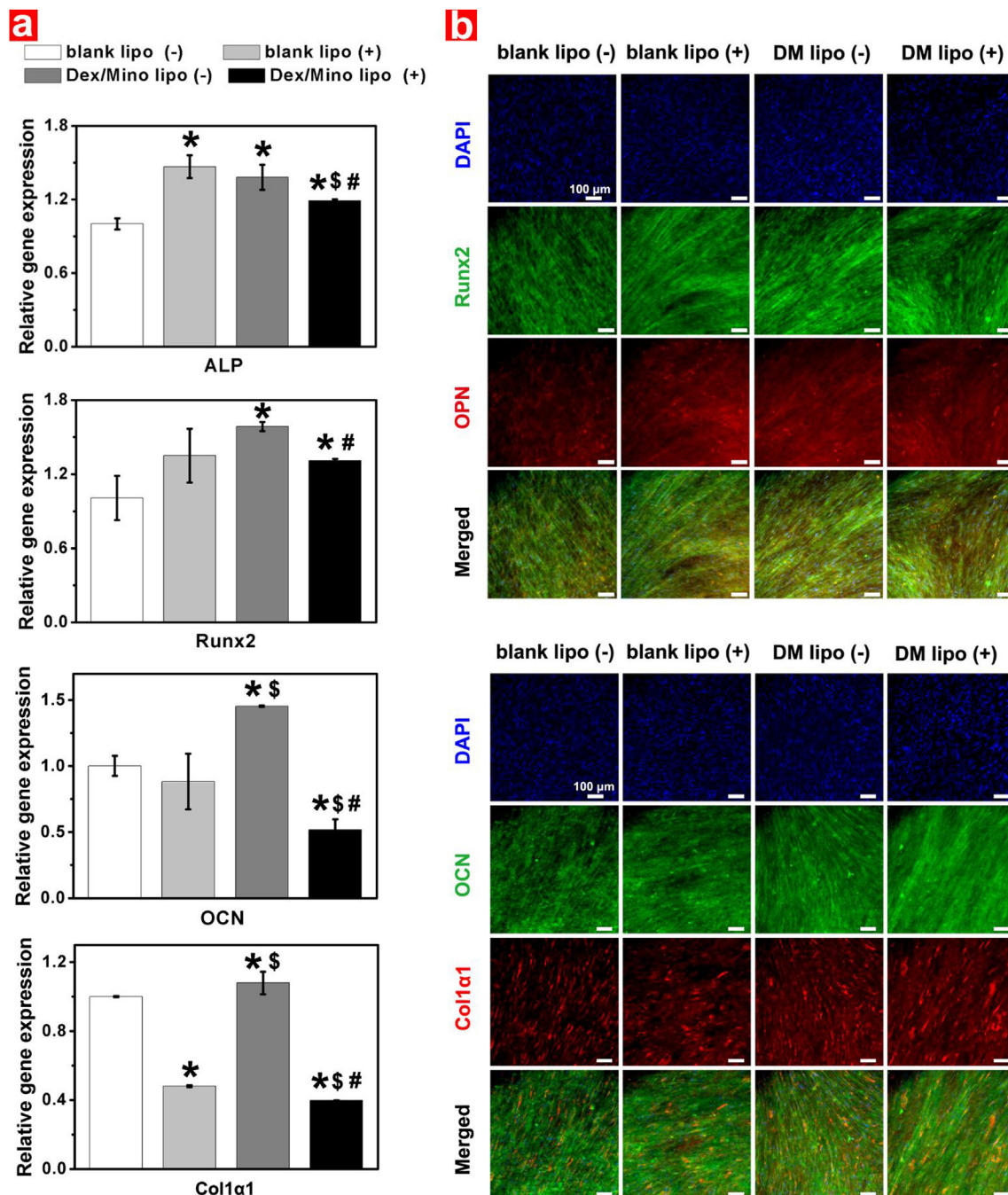


**Fig. 5.** Osteogenic marker expression in hMSCs cultured on liposome-modified polystyrene surfaces on day 14. (a) RT-PCR analysis of osteo-related genes encoding ALP, Runx 2, OCN, and Col1α1. \*, \$, #:  $p < 0.05$  compared with blank lipo (-), blank lipo (+), and Dex/Mino lipo (-), respectively. All data represent the mean  $\pm$  SD ( $n = 6$ ). (b) Representative immunofluorescent images of Runx2, OPN, OCN, and Col1α1 in different groups. Runx2 and OCN are labeled by green fluorescence, whereas OPN and Col1α1 are marked by red fluorescence. The cells were counterstained with DAPI for nuclei in blue. The + and - symbols refer to Dex-existent osteogenic differentiation medium (also called the osteoinductive medium) and Dex-absent osteogenic differentiation medium (also called the osteoconductive medium), respectively. Abbreviations: ALP, alkaline phosphate; Col1α1, rabbit polyclonal antihuman Type I collagen alpha 1; DAPI, 4',6-diamidino-2-phenylindole; OCN, mouse monoclonal antihuman osteocalcin; OPN, rabbit monoclonal antihuman osteopontin; Runx2, mouse monoclonal antihuman Runt-related transcription factor 2.

possibly directly ingesting Dex/Mino liposomes in the intracellular space [53].

### 3.4. Enhanced osteogenic differentiation of hMSCs grown on Dex/Mino liposome-decorated PEEK surfaces under both the osteoinductive and osteoconductive conditions

In terms of implant materials, a crucial factor in new bone

regeneration is the osteogenic differentiation capacity of hMSCs on the implant surfaces. The results above demonstrate that our surface modification strategy could be useful for the biofunctionalization of implant biomaterials. In this section, we applied this strategy to the PEEK surface treatment, verifying the capacity of liposomal Dex to promote osteogenic differentiation of hMSCs.

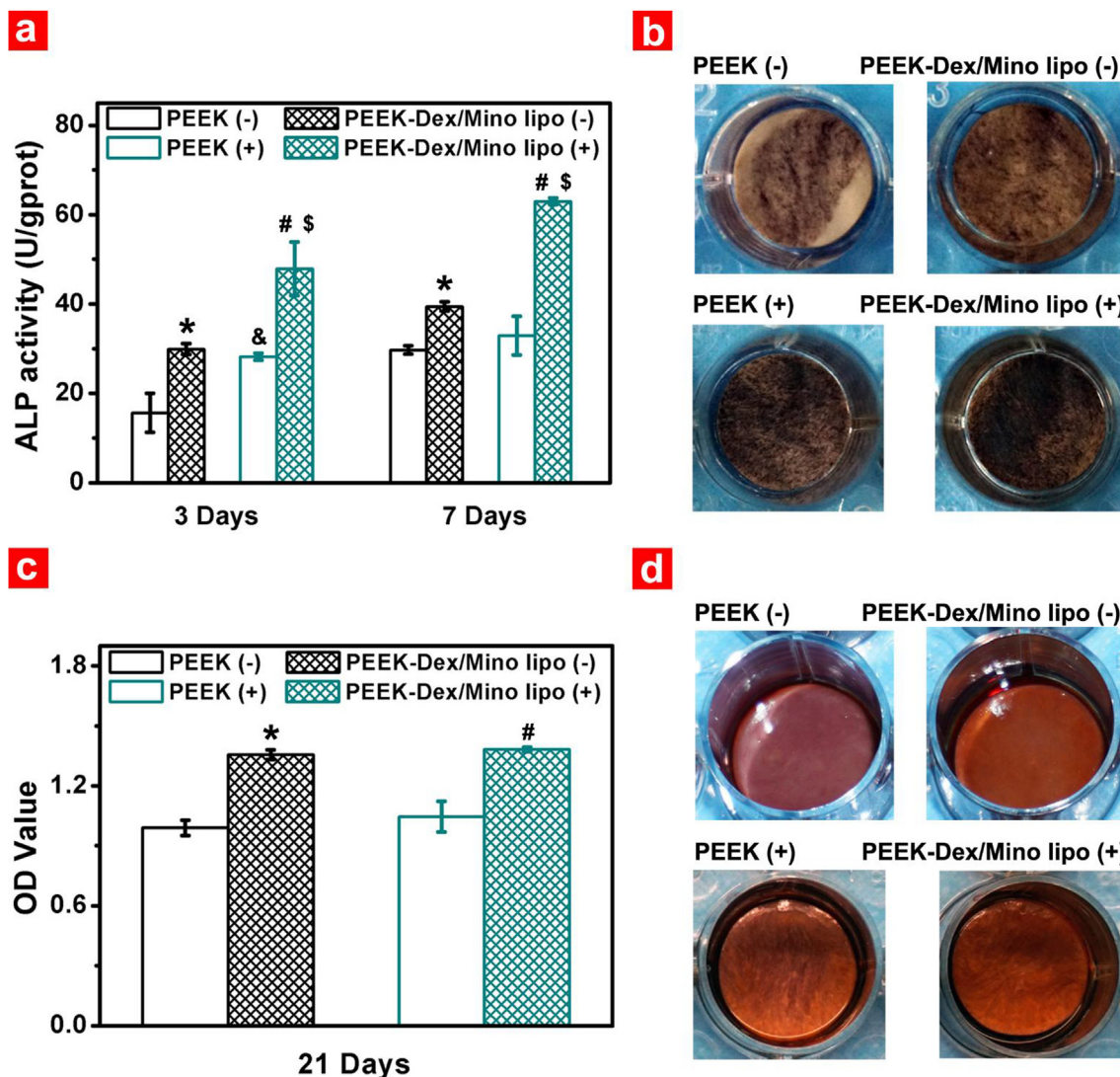


**Fig. 6.** The effect of Dex/Mino liposome-functionalized PEEK surfaces on osteogenic differentiation of hMSCs under the osteoinductive and osteoconductive condition. (a) Determination of ALP activity at 3 and 7 days and (b) representative staining of ALP on day 7. (c) Determination of calcium deposition at 21 days and (d) Alizarin Red S staining on day 21. \*: Significant difference between the PEEK (-) and the PEEK-Dex/Mino lipo (-) groups ( $p < 0.05$ ). #: Significant difference between the PEEK (+) and the PEEK-Dex/Mino lipo (+) groups ( $p < 0.05$ ). \$: Significant difference between the PEEK-Dex/Mino lipo (-) and the PEEK-Dex/Mino lipo (+) groups ( $p < 0.05$ ). &: Significant difference between the PEEK (-) and the PEEK (+) groups ( $p < 0.05$ ). All data represent the mean  $\pm$  SD ( $n = 6$ ). The + refers to osteoinductive medium (also called the Dex-existent osteogenic differentiation medium). The - symbol refers to osteoconductive medium (also called the Dex-absent osteogenic differentiation medium).

### 3.4.1. Osteogenic differentiation evaluation under osteoinductive condition

Dex, as noted above, enhances the osteogenic differentiation activity of hMSCs. We rationally deduced that the release of Dex from Dex/Mino liposome-modified PEEK might enable higher osteoblastic differentiation than single use of osteoinductive medium. Hence, we compared the osteogenic differentiation capacity of hMSCs that were cultured separately with bare PEEK and Dex/Mino liposome-decorated PEEK under osteoinductive condition. The + refers to osteoinductive medium (also called the Dex-existent osteogenic differentiation medium).

ALP quantification was performed at 3 and 7 days to assess the *in vitro* ALP activity of hMSCs incubated with PEEK (+) and PEEK-Dex/Mino lipo (+) (Fig. 6a); both groups showed good time-dependent ALP expression. The PEEK-Dex/Mino lipo (+) group showed higher expression of ALP than the bare PEEK (+) group at days 3 and 7, suggesting that modification of the liposomal Dex on the PEEK surface effectively enhanced osteogenic differentiation of the hMSCs under the osteoinductive condition. Notably, the ALP activity of the PEEK-Dex/Mino

lipo (+) group was more than 1.9-fold higher than that of the PEEK (+) group on day 7, underlining an effective synergistic influence on the osteogenic differentiation of hMSCs between the Dex presented in osteoinductive medium and the liposomal Dex released from the functionalized PEEK surface. ALP staining at day 7 (Fig. 6b) was also performed. The ALP-positive areas were visibly larger on the PEEK-Dex/Mino lipo (+) surface than on the PEEK (+) surface, which is in good agreement with the quantitative results.

Alizarin Red S staining was further performed on day 21 to assess the mineralized matrix synthesis in osteoinductive medium. Calcium deposition was quantified (Fig. 6c). A moderate increase in calcium deposition was found when cells were incubated on PEEK-Dex/Mino lipo (+) compared with hMSCs incubated on PEEK (+). Fig. 6d shows that the hMSCs incubated on the PEEK-Dex/Mino lipo (+) surface displayed obviously denser and larger red staining (typical for calcium deposition) than the PEEK (+) group, indicating that the liposomal Dex coating may promote osteogenic differentiation. The enhancement in efficiency of mineralization after Dex loading suggested that Dex/Mino

liposome modification could effectively improve the osteogenic differentiation activity of bioinert PEEK materials under the osteoinductive condition. Taken together, the good osteogenic properties of Dex/Mino liposome-decorated PEEK may result in faster osseointegration at the interfaces between implants and the bone tissues.

### 3.4.2. Osteogenic differentiation evaluation under osteoconductive condition

Considering the spontaneous osteogenic differentiation of hMSCs in the presence of osteoinductive factors (including Dex, ascorbic acid, and  $\beta$ -glycerophosphate), we simultaneously analyzed the differentiation of hMSCs in Dex-absent osteogenic medium (also called the osteoconductive medium), to avoid the disturbance of Dex seen in the osteoinductive medium and thereby disclose the intrinsic osteogenic activity of Dex/Mino liposome-functionalized PEEK. The – symbol refers to osteoconductive medium (also called the Dex-absent osteogenic differentiation medium).

Fig. 6 also shows that hMSCs on the bare PEEK (–) surface expressed low ALP activity after 3 and 7 days of cultivation, and produced few calcium nodules at day 21, indicating a poorly differentiated state under the osteoconductive condition because of the absence of soluble osteoinducing Dex. Nevertheless, when Dex/Mino liposomes were coated onto the bioinert PEEK surface, a remarkable reinforcement of ALP activity was found on PEEK-Dex/Mino lipo (–) group in hMSCs after both 3 and 7 days of incubation, despite the weakened expression under the osteoconductive condition (Fig. 6a and b). ARS quantification and staining showed a similar behavior. The PEEK-Dex/Mino lipo (–) group showed higher expression of calcium deposition than the bare PEEK (–) group at day 21 (Fig. 6c). Compared with the PEEK (–) control, more calcium nodules were observed when hMSCs were cultured on the PEEK-Dex/Mino lipo (–) surface for 21 days (Fig. 6d). Overall, Dex released from liposome-decorated PEEK surfaces instead of soluble osteoinducing Dex effectively promoted osteogenic differentiation of hMSCs in the osteoconductive condition. Moreover, although the ALP activity of hMSCs cultured on Dex/Mino liposome-modified PEEK surfaces in the osteoconductive medium was not comparable to that in the osteoinductive medium, the application of Dex/Mino liposomes effectively activated the osteogenic activity of hMSCs despite the absence of soluble osteoinducing Dex.

### 3.5. In vitro and in vivo bacteriostasis assays

A bacteriostatic implant surface is essential because the interface between the implant surface and surrounding tissue is susceptible to bacterial attack, and postoperative implantation failure may occur if infection is not controlled [54]. A crucial factor in infection is the initial adhesion of bacteria onto implant interfaces, which is also a primary component of biofilm formation [55]. Considering the enduring success of implants, it is crucial to block bacterial adhesion to implanted biomaterials during the initial stage of postoperative implantation. It is well-established that *P. gingivalis* is a pivotal pathogenic microbe related to peri-implantitis, and that *S. mutans* is an important and widely studied early colonizer involved in dental biofilms (plaques) [56,57]. In the present research, both Gram-negative *P. gingivalis* and Gram-positive *S. mutans* were selected to evaluate the bacteriostatic effect of the Dex/Mino liposome-decorated PEEK surfaces *in vitro* and *in vivo*.

Fig. 7a shows changes in the amount and viability of both *P. gingivalis* and *S. mutans*. In the initial adhesion phase (4 h), almost no *P. gingivalis* was detected on both sample surfaces. Compared with that of the pristine PEEK group, fewer *S. mutans* were observed on the PEEK-Dex/Mino lipo group, implying the positive bacteriostatic effect of liposomal Mino releasing. At the proliferation stage (24 h), the number of both bacteria increased with increasing incubation time on the bare PEEK surface; conversely, the PEEK-Dex/Mino lipo group presented a slight increase in the amount of *P. gingivalis* and no growth in the amount of *S. mutans*. Moreover, fewer *P. gingivalis* and *S. mutans* were

observed on the PEEK-Dex/Mino lipo group versus that of the bare PEEK group. Accordingly, we inferred that Mino releasing from Dex/Mino liposome-modified PEEK surfaces effectively prevented bacterial adhesion and proliferation. Fig. 7b provides live/dead fluorescent images of *P. gingivalis* and *S. mutans* cultured for 24 h on different PEEK surfaces. There are clearly more live bacteria (both *P. gingivalis* and *S. mutans*) appearing as green fluorescence on the bare PEEK than on the Dex/Mino liposome-modified PEEK, which is congruent with the results of microbial viability quantification. These findings hinted at the inability of bare PEEK to inhibit bacteria, but the adoption of Dex/Mino liposome improved the antibacterial activity of bioinert PEEK against *P. gingivalis* and *S. mutans*.

We further subcutaneously implanted Dex/Mino liposome-functionalized PEEK into C57BL/6 mice to assess the antibacterial activity *in vivo*. The live bacteria colonies harvested from tissue fluid are shown in Fig. 7c and d. The bacterial colony counts for the PEEK and Dex/Mino liposome-modified PEEK were  $77 \pm 44$  and  $2 \pm 1$ , respectively. Compared with the bare PEEK, fewer live bacterial colonies were observed on the Dex/Mino liposome-modified PEEK, which was consistent with the results of the *in vitro* study. Furthermore, we estimated that the antibacterial efficiency of Dex/Mino liposome-modified PEEK was about 97.4% against *S. mutans*, which proved its effective bacteriostasis *in vivo*.

Mino is an antibacterial agent that exerts its effects by interfering with the synthesis of bacterial protein. The mechanism by which Mino may block bacterial peptide and ribosomal protein synthesis can be summarized as breaking the association of aminoacyl-tRNA and bacterial ribosome by combining to form a specific ribosomal subunit, thereby disintegrating bacterial cells [58]. As far as implantation is concerned, a race between bacterial adhesion and cell adhesion on the biomaterial surface decides the implant outcome [59,60]. Ideal implantation should ensure that tissue integration precedes bacterial adhesion, thus guarding against bacterial multiplication on the implant interface. Both benign cell adhesion on the functionalized PEEK surface and liposomal Mino releasing may exert a positive impact on the bacteriostatic effect of the Dex/Mino liposome-modified PEEK, through turning the “run for the surface” toward the cells and against the bacteria. Taken together, the bacteriostatic effect of pristine PEEK was improved by introducing Dex/Mino liposome modification, which may be significant in preventing implant-associated infections.

### 3.6. In vivo anti-inflammation analysis

Besides being an osteoinducing factor, Dex as a glucocorticoid is also broadly applied to attenuate inflammation in different clinical conditions, but with severe side-effects [61]. The local delivery of glucocorticoids by liposomes could be beneficial in reducing the side-effects of various therapies [62,63]. In the present research, we used a subcutaneous implant-associated inflammatory reaction model to evaluate whether the release of Dex from liposomes could ease the foreign body response to PEEK implants. Typical tissue sections stained with HE are displayed in Fig. S8. It is well-known that the emergence of inflammatory cells indicates a foreign body reaction in the early phase [64]. After 1 day of implantation, a strong inflammatory cell infiltration induced by surgical trauma and foreign body response was found in the bare PEEK group. In contrast, milder cell infiltration was observed with functionalized PEEK, indicating an effective anti-inflammatory action of releasing Dex from the liposomes. We further examined proinflammatory cytokine (TNF- $\alpha$  and IL-6) levels after subcutaneous implantation in a C57BL/6 mouse for 1 day. The ELISA (Fig. 8) revealed that, compared with the bare PEEK group, the release of proinflammatory mediators was obviously lower in the Dex/Mino liposome-modified group; this was consistent with the corresponding HE staining analysis. Although the host innate immunity is indispensable in this circumstance, previous research has emphasized that immunosuppressive status or impaired immune function would render the

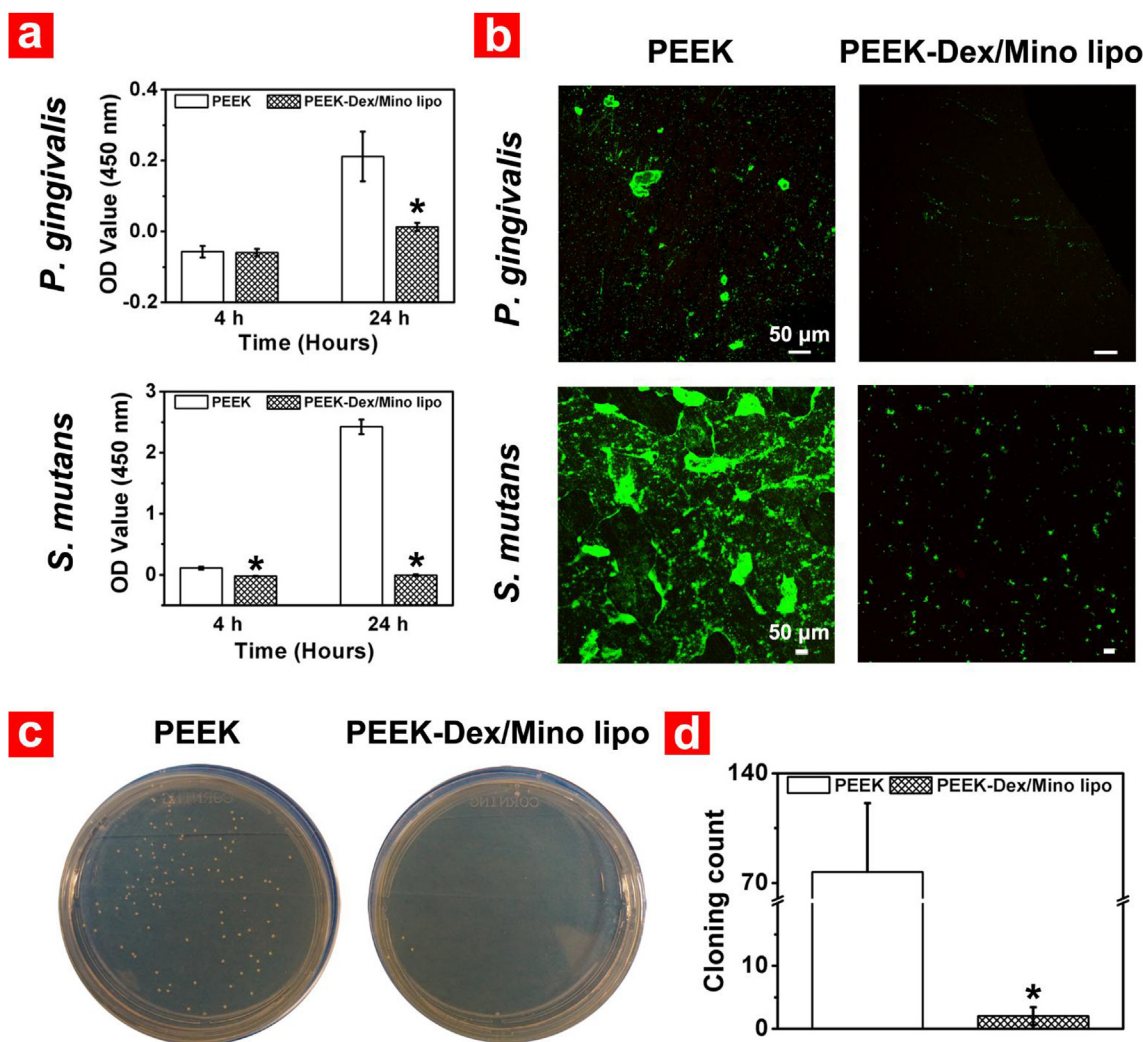


**Fig. 7.** *In vitro* and *in vivo* antibacterial and histological evaluations. (a) *In vitro* antibacterial activity of functionalized PEEK sample against Gram-negative *P. gingivalis* and Gram-positive *S. mutans* cultured for 4 and 24 h \*:  $p < 0.05$  when compared with the PEEK group. All data represent the mean  $\pm$  SD (n = 9). (b) Live/dead fluorescent images of *P. gingivalis* and *S. mutans* adhered after 24 h of incubation. (c) Representative images of the agar plates for the colonies of *S. mutans* extracted from the subcutaneous tissue after implantation for 24 h. (d) Quantitative results of *S. mutans* colonies in the agar plate samples. \*:  $p < 0.05$  compared with the PEEK group. All data represent the mean  $\pm$  SD (n = 3).

host less able to resist inflammation and infection [65]. Therefore, it is important to develop a PEEK implant that is equipped to release Dex, to control the foreign body reaction. Overall, this subcutaneous implantation assay confirmed that the release of Dex from the liposome-modified PEEK surface could alleviate the inflammatory response post-implantation.

### 3.7. *In vivo* new bone formation study

The *in vitro* osteogenic activity assay suggested that the Dex/Mino liposome-decorated surfaces boosted the osteogenesis of pristine PEEK. The *in vivo* tissue response to the Dex/Mino liposome-decorated PEEK, as one of the crucial indicators of osseointegration, was also studied in this research. This is closely correlated with our material becoming an artificial implant. We created a beagle femur implantation model for a

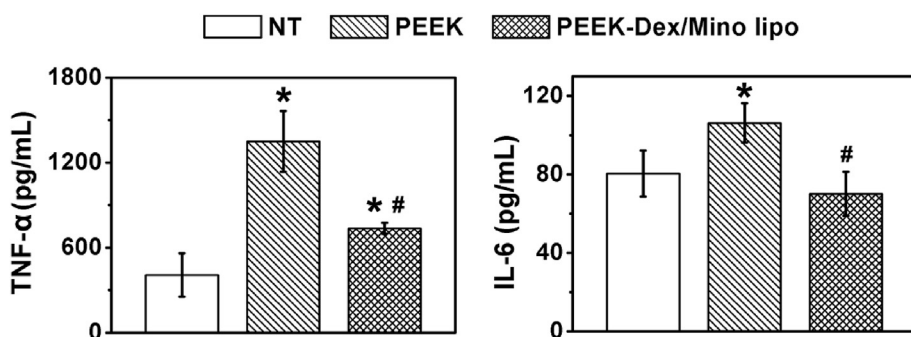


**Fig. 8.** *In vivo* evaluation of the subcutaneous implant-associated inflammatory reaction. ELISA from subcutaneous implant samples show protein expression of inflammatory markers (TNF- $\alpha$  and IL-6) at day 1. \*, #:  $p < 0.05$  compared with NT and PEEK, respectively. All data represent the mean  $\pm$  SD (n = 6). Abbreviations: ELISA, enzyme-linked immunosorbent assay; IL-6, interleukin-6; NT, normal tissue; TNF- $\alpha$ , tumor necrosis factor- $\alpha$ .

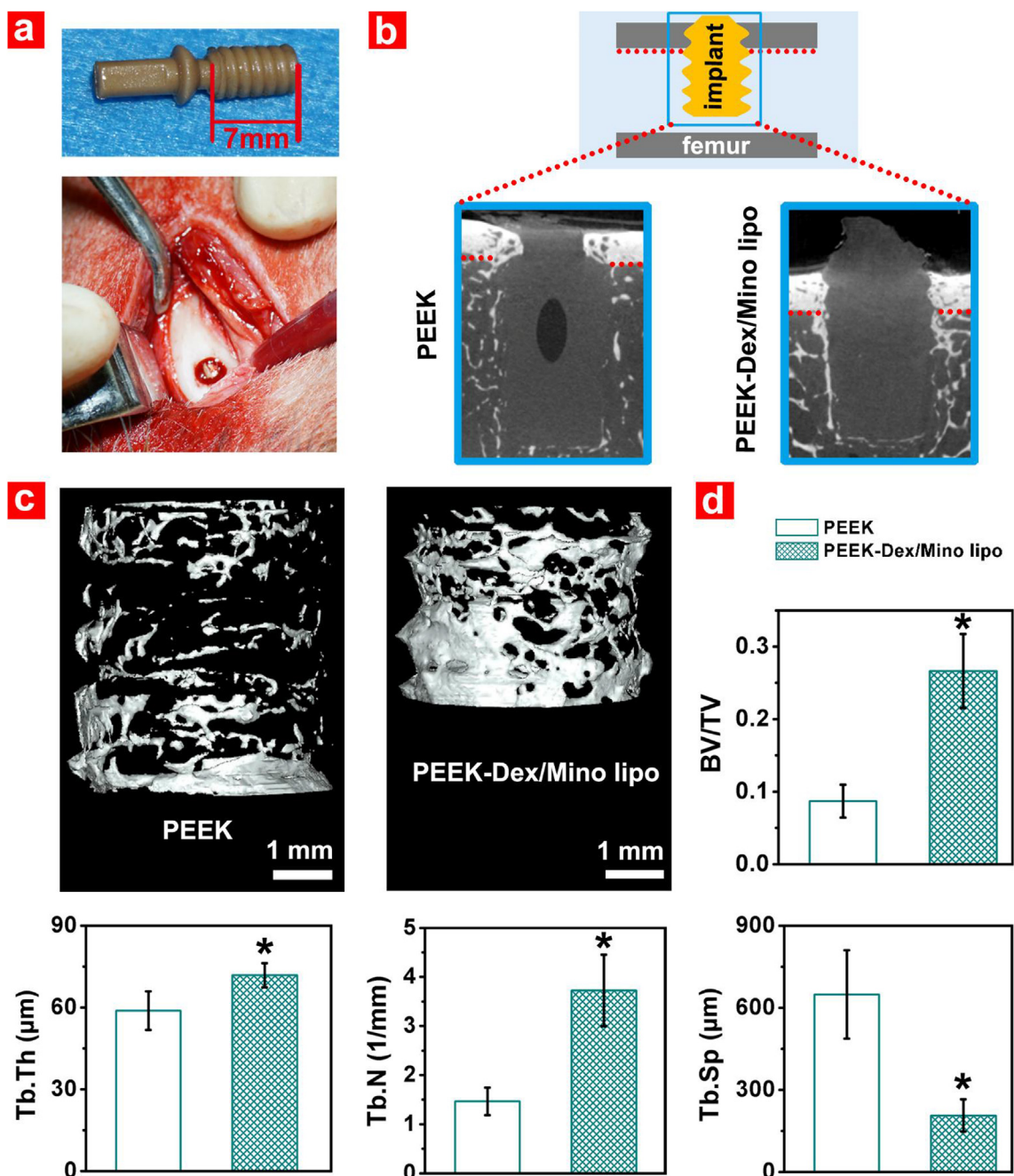


Fig. 9. Micro-CT analysis of the experimental coatings *in vivo* new bone formation. (a) Macroscopic images of Dex/Mino liposome-modified PEEK implant and a beagle's femur containing an implant. (b) Schematic and micro-CT images of vertical beagle femur sections with implants after 8 weeks of implantation. (c) Micro-CT 3D reconstruction images and (d) quantitative analysis of the samples after 8 weeks of implantation. \*:  $p < 0.05$  compared with the PEEK group. All data represent the mean  $\pm$  SD ( $n = 5$ ).

more convincing demonstration; a functionalized PEEK implant was implanted into the femoral marrow cavity (Fig. 9a).

### 3.7.1. Micro-CT assay

At 8 weeks after surgery, we extracted and evaluated bone specimens using micro-CT. This technique provided both high-resolution 2D/3D images and bone histomorphometry indices showing detailed bone formation around the implant and changes in new bone formation. Fig. 9b shows vertical sections and 2D CT images of the newly formed bone around the implants in the bone marrow cavity. We focused on the areas below the red dotted line and found that the new bone volume around the surface of the Dex/Mino liposome-modified PEEK implant was clearly higher than that around the PEEK implant

under the cortical bone. Inconsecutive parts of adjacent bone around the implanted pristine PEEK were noted in 3D reconstruction images, and more formation of new bone was seen around the Dex/Mino liposome-decorated PEEK compared with the bare PEEK counterpart (Fig. 9c). The quantitative analyses of bone volume/total volume (BV/TV), trabecular thickness (Tb.Th), trabecular number (Tb.N), and trabecular separation (Tb.Sp) are shown in Fig. 9d. The BV/TV for the PEEK-Dex/Mino lipo implant group was significantly higher than that for the pristine PEEK control. Higher Tb.Th and Tb.N values were also found for the PEEK-Dex/Mino lipo implant group than for the pure PEEK implant group. Additionally, compared with the PEEK implant, the PEEK-Dex/Mino lipo implant had a lower Tb.Sp. Previous studies have shown that osseointegration direct osteoblast colonization on an

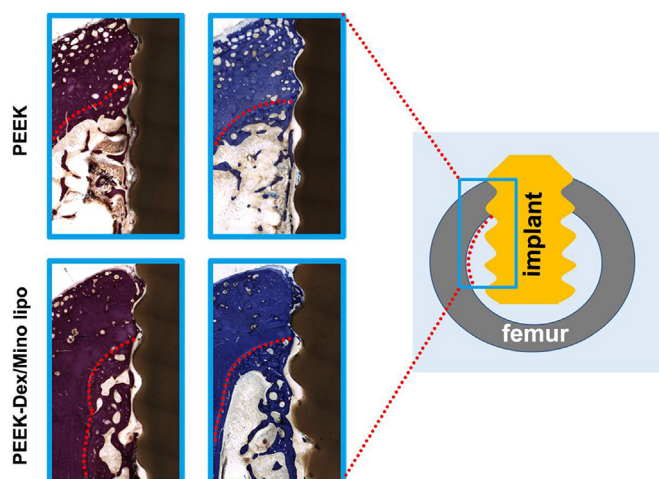


**Fig. 10.** Histological analysis of the experimental coatings *in vivo* osseointegration. Schematic illustration of the transverse perspective. The histological sections were processed by HE staining (left) and toluidine blue staining (right). The blue rectangles are displayed as partial magnifications of the area in schematic. Abbreviations: HE, hematoxylin and eosin.

implant surface, synthesizing extracellular bone matrix and finally forming new bone [49,66]. The results above indicate that PEEK with the Dex/Mino liposome coating significantly enhanced new bone formation compared with the pristine PEEK control, which corresponded to the proliferation and osteogenic differentiation of hMSCs *in vitro*. Previous studies reported that Dex modification of nanoparticles or nanofibers yielded higher osteo-related protein expression and calcified bone formation [67,68]. After implantation of PEEK with the Dex/Mino liposome coating, the release of liposomal Dex necessarily boosted osteoblast growth in the bone marrow, finally resulting in new bone regeneration. Hence, functionalized PEEK, after modification with liposomal Dex, enhanced new bone formation around the implant and further promoted ossification between the implant and the bone. These findings confirm that the Dex/Mino liposome-decorated PEEK favored the improvement of *in vivo* osseointegration.

### 3.7.2. Histological analysis

Histological sections were processed by HE staining and toluidine blue staining after 8 weeks of implantation (Fig. 10). The HE staining revealed fragments of new bone next to the bare PEEK implant surface, and a larger gap between the sample and new bone tissue was evident compared with the functionalized PEEK. However, in the PEEK-Dex/Mino lipo group, the new bone formation was greater than in the PEEK control, firmly anchoring onto the modified surface and extending along the implant interface. The toluidine blue staining showed only a few bits of new bone discontinuously dispersed around the bare PEEK implant. In contrast, the Dex/Mino liposome-modified PEEK promoted a larger area of new bone formation. The newly formed bone grew from the parent bone into the marrow cavity and extended along the implant interface, which was in good agreement with the micro-CT and HE staining results. Accordingly, the samples having the pDA-mediated Dex/Mino liposome modification effectively sped up bone deposition and boosted ossification of the PEEK interface. Taken together, the various *in vivo* studies suggest that our Dex/Mino liposome-modified PEEK implant is able to bond with host bones and enhance new bone formation, which is favorable behavior for orthopedic/dental implants. Furthermore, the *in vivo* and *in vitro* results are consistent, suggesting that the introduction of the Dex/Mino liposomes modification is necessary for PEEK osseointegration.

## 4. Conclusions

We established that a Dex/Mino liposome-modified PEEK surface was endowed with bacteriostatic, anti-inflammatory, and osteogenic capabilities. Our facile surface coating method and the remarkable biological functions developed for the bio-functionalization of a PEEK implant show great clinical promise. Our multifunctional PEEK was effective at repairing bone defects by virtue of its favorable biocompatibility and enhanced osteogenesis. Additionally, the introduction of Dex/Mino liposomes contributed to decreased systemic toxicity and antibiotic resistance, and improved the local anti-inflammatory and bacteriostasis effectiveness of the implants. We consider that this multifunctional PEEK is highly suitable for orthopedic/dental applications and has great clinical potential.

## 5. Supplementary data

Pristine and functionalized PEEK samples; Dex/Mino liposome formulations and schematic diagram of the preparation of Dex/Mino liposome-decorated PEEK through pDA coating, as well as its bacteriostasis and anti-inflammatory and osseointegrative properties *in vitro* and *in vivo*; fluorescently labeled liposomes attached to PEEK-NF-lipo and PEEK-lipo substrates and their semiquantitative results; XPS scan spectra of PEEK-NF-Dex/Mino lipo (P 2p and P 2s), PEEK-pDA, and PEEK-Dex/Mino lipo before and after immersion in PBS for 7 and 14 days; AFM image and the surface roughness of the PEEK-NF-Dex/Mino lipo sample; CLSM and SEM observations of adhering hMSCs cultured on different PEEK surfaces for 1 day; histological evaluation of the subcutaneous implant-associated inflammatory reaction; primer sequences used for RT-PCR analysis; elemental composition of different PEEK surfaces determined by XPS analysis; the antibacterial efficiency of Dex/Mino liposome-modified PEEK against *S. mutans* cultured for 4 and 24 h.

## Author Contributions

This manuscript was written by all authors listed, who agreed on the final manuscript. The authors declare no competing interest.

## 6. Notes

In each group, 3–6 different areas were randomly selected to take the images (including fluorescent images, SEM/AFM images, and ALP/ARS staining images), and we exhibited the most representative one. The English in this document has been checked by at least two professional editors, both native speakers of English. For a certificate, please see: <http://www.textcheck.com/certificate/SmYrJn>.

## Acknowledgments

This work was supported by the National Natural Science Foundation of China (No. 81571814) and National Key Research and Development Program of China (No. 2016YFC1102104). We thank Hao Liu and Rui Shi (Central Laboratory, School and Hospital of Stomatology, Peking University) for their help with micro CT and histological assays. We thank Ziqian Zeng (Department of Oral and Maxillofacial Surgery, School and Hospital of Stomatology, Peking University) for his assistance in operating subcutaneous implantation.

## Appendix A. Supplementary data

Supplementary data to this article can be found online at <https://doi.org/10.1016/j.biomaterials.2019.05.014>.

## References

- [1] J. Yan, C. Wang, K. Li, Q. Zhang, M. Yang, W. Di-Wu, M. Yan, Y. Song, J. Ba, L. Bi, Y. Han, Enhancement of surface bioactivity on carbon fiber-reinforced polyether ether ketone via graphene modification, *Int. J. Nanomedicine* 13 (2018) 3425–3440.
- [2] T. Lu, J. Wen, S. Qian, H. Cao, C. Ning, X. Pan, X. Jiang, X. Liu, P.K. Chu, Enhanced osteointegration on tantalum-implanted polyetheretherketone surface with bone-like elastic modulus, *Biomaterials* 51 (2015) 173–183.
- [3] J.H. Lee, H.L. Jang, K.M. Lee, H.R. Baek, K. Jin, K.S. Hong, J.H. Noh, H.K. Lee, *In vitro* and *in vivo* evaluation of the bioactivity of hydroxyapatite-coated polyetheretherketone biocomposites created by cold spray technology, *Acta Biomater.* 9 (2013) 6177–6187.
- [4] C.M. Han, E.J. Lee, H.E. Kim, Y.H. Koh, K.N. Kim, Y. Ha, S.U. Kuh, The electron beam deposition of titanium on polyetheretherketone (PEEK) and the resulting enhanced biological properties, *Biomaterials* 31 (2010) 3465–3470.
- [5] R.D. Carpenter, B.S. Klosterhoff, F.B. Torstrick, K.T. Foley, J.K. Burkus, C.S.D. Lee, K. Gall, R.E. Guldberg, D.L. Safranski, Effect of porous orthopaedic implant material and structure on load sharing with simulated bone ingrowth: a finite element analysis comparing titanium and PEEK, *J. Mech. Behav. Biomed. Mater.* 80 (2018) 68–76.
- [6] S. Najeeb, M.S. Zafar, Z. Khurshid, F. Siddiqui, Applications of polyetheretherketone (PEEK) in oral implantology and prosthodontics, *J. Prosthodont. Res.* 60 (2016) 12–19.
- [7] T. Lu, X. Liu, S. Qian, H. Cao, Y. Qiao, Y. Mei, P.K. Chu, C. Ding, Multilevel surface engineering of nanostructured TiO<sub>2</sub> on carbon-fiber-reinforced polyetheretherketone, *Biomaterials* 35 (2014) 5731–5740.
- [8] Y. Zhao, H.M. Wong, W. Wang, P. Li, Z. Xu, E.Y.W. Chong, C.H. Yan, K.W.K. Yeung, P.K. Chu, Cytocompatibility, osseointegration, and bioactivity of three-dimensional porous and nanostructured network on polyetheretherketone, *Biomaterials* 34 (2013) 9264–9277.
- [9] Z. Sun, L. Ouyang, X. Ma, Y. Qiao, X. Liu, Controllable and durable release of BMP-2-loaded 3D porous sulfonated polyetheretherketone (PEEK) for osteogenic activity enhancement, *Colloids Surf. B Biointerfaces* 171 (2018) 668–674.
- [10] S. Liu, Y. Zhu, H. Gao, P. Ge, K. Ren, J. Gao, Y. Cao, D. Han, J. Zhang, One-step fabrication of functionalized poly(etheretherketone) surfaces with enhanced biocompatibility and osteogenic activity, *Mater. Sci. Eng. C Mater. Biol. Appl.* 88 (2018) 70–78.
- [11] R. Ma, S. Tang, H. Tan, J. Qian, W. Lin, Y. Wang, C. Liu, J. Wei, T. Tang, Preparation, characterization, *in vitro* bioactivity, and cellular responses to a polyetheretherketone bioactive composite containing nanocalcium silicate for bone repair, *ACS Appl. Mater. Interfaces* 6 (2014) 12214–12225.
- [12] T. Albrektsson, C. Johansson, Osteoinduction, osteoconduction and osseointegration, *Eur. Spine J.* 10 (2001) S96–S101.
- [13] B. Yuan, Q. Cheng, R. Zhao, X. Zhu, X. Yang, X. Yang, K. Zhang, Y. Song, X. Zhang, Comparison of osteointegration property between PEKK and PEEK: effects of surface structure and chemistry, *Biomaterials* 170 (2018) 116–126.
- [14] F.B. Torstrick, A.S.P. Lin, D. Potter, D.L. Safranski, T.A. Sulchek, K. Gall, R.E. Guldberg, Porous PEEK improves the bone-implant interface compared to plasma-sprayed titanium coating on PEEK, *Biomaterials* 185 (2018) 106–116.
- [15] R. Ma, Z. Yu, S. Tang, Y. Pan, J. Wei, T. Tang, Osseointegration of nanohydroxyapatite- or nanocalcium silicate-incorporated polyetheretherketone bioactive composites *in vivo*, *Int. J. Nanomedicine* 11 (2016) 6023–6033.
- [16] D.W. Lee, Y.P. Yun, K. Park, S.E. Kim, Gentamicin and bone morphogenic protein-2 (BMP-2)-delivering heparinized-titanium implant with enhanced antibacterial activity and osteointegration, *Bone* 50 (2012) 974–982.
- [17] W. Zhou, Z. Jia, P. Xiong, J. Yan, Y. Li, M. Li, Y. Cheng, Y. Zheng, Bioinspired and biomimetic AgNPs/gentamicin-embedded silk fibroin coatings for robust antibacterial and osteogenic applications, *ACS Appl. Mater. Interfaces* 9 (2017) 25830–25846.
- [18] L. Wang, S. He, X. Wu, S. Liang, Z. Mu, J. Wei, F. Deng, Y. Deng, S. Wei, Polyetheretherketone/nano-fluorohydroxyapatite composite with antimicrobial activity and osseointegration properties, *Biomaterials* 35 (2014) 6758–6775.
- [19] B.N. Brown, S.F. Badylak, Expanded applications, shifting paradigms and an improved understanding of host-biomaterial interactions, *Acta Biomater.* 9 (2013) 4948–4955.
- [20] F. Bensiamar, B. Olalde, S.C. Cifuentes, N. Argarate, G. Atorrasagasti, J.L. González-Carrasco, E. García-Rey, N. Vilaboa, L. Saldaña, Bioactivity of dexamethasone-releasing coatings on polymer/magnesium composites, *Biomed. Mater.* 11 (No) (2016) 055011.
- [21] J.M. Anderson, A. Rodriguez, D.T. Chang, Foreign body reaction to biomaterials, *Semin. Immunol.* 20 (2008) 86–100.
- [22] S.B. Goodman, Z. Yao, M. Keeney, F. Yang, The future of biologic coatings for orthopaedic implants, *Biomaterials* 34 (2013) 3174–3183.
- [23] Y. Zheng, L. Liu, L. Xiao, Q. Zhang, Y. Liu, Enhanced osteogenic activity of phosphorylated polyetheretherketone via surface-initiated grafting polymerization of vinylphosphonic acid, *Colloids Surf. B Biointerfaces* 173 (2019) 591–598.
- [24] R. Ma, T. Tang, Current strategies to improve the bioactivity of PEEK, *Int. J. Mol. Sci.* 15 (2014) 5426–5445.
- [25] G. Pezzotti, E. Marin, T. Adachi, F. Lerusi, A. Rondinella, F. Boschetto, W. Zhu, T. Kitajima, K. Inada, B.J. McEntire, R.M. Bock, B.S. Bal, O. Mazda, Incorporating Si<sub>3</sub>N<sub>4</sub> into PEEK to produce antibacterial, osteoconductive, and radiolucent spinal implants, *Macromol. Biosci.* 18 (2018) e1800033.
- [26] X. Liu, P.K. Chu, C. Ding, Surface nano-functionalization of biomaterials, *Mater. Sci. Eng. R* 70 (2010) 275–302.
- [27] J. Wu, L. Li, C. Fu, F. Yang, Z. Jiao, X. Shi, Y. Ito, Z. Wang, Q. Liu, P. Zhang, Microporous polyetheretherketone implants decorated with BMP-2 via phosphorylated gelatin coating for enhancing cell adhesion and osteogenic differentiation, *Colloids Surf. B Biointerfaces* 169 (2018) 233–241.
- [28] H. Mahjoubi, E. Buck, P. Manimunda, R. Farivar, R. Chromik, M. Murshed, M. Cerruti, Surface phosphonation enhances hydroxyapatite coating adhesion on polyetheretherketone and its osseointegration potential, *Acta Biomater.* 47 (2017) 149–158.
- [29] T. Shimizu, S. Fujibayashi, S. Yamaguchi, K. Yamamoto, B. Otsuki, M. Takemoto, M. Tsukanaka, T. Kizuki, T. Matsushita, T. Kokubo, S. Matsuda, Bioactivity of sol-gel-derived TiO<sub>2</sub> coating on polyetheretherketone: *in vitro* and *in vivo* studies, *Acta Biomater.* 35 (2016) 305–317.
- [30] S. Spriano, S. Yamaguchi, F. Bano, S. Ferraris, A critical review of multifunctional titanium surfaces: new frontiers for improving osseointegration and host response, avoiding bacteria contamination, *Acta Biomater.* 79 (2018) 1–22.
- [31] X. Yuan, L. Ouyang, Y. Luo, Z. Sun, C. Yang, J. Wang, X. Liu, X. Zhang, Multifunctional sulfonated polyetheretherketone coating with beta-defensin-14 for yielding durable and broad-spectrum antibacterial activity and osseointegration, *Acta Biomater.* 86 (2019) 323–337.
- [32] L. Deng, X. He, K. Xie, L. Xie, Y. Deng, Dual therapy coating on micro/nanoscale porous polyetheretherketone to eradicate biofilms and accelerate bone tissue repair, *Macromol. Biosci.* 19 (2019) e1800376.
- [33] J. Yan, W. Zhou, Z. Jia, P. Xiong, Y. Li, P. Wang, Q. Li, Y. Cheng, Y. Zheng, Endowing polyetheretherketone with synergistic bactericidal effects and improved osteogenic ability, *Acta Biomater.* 79 (2018) 216–229.
- [34] M. Liu, G. Zeng, K. Wang, Q. Wan, L. Tao, X. Zhang, Y. Wei, Recent developments in polydopamine: an emerging soft matter for surface modification and biomedical applications, *Nanoscale* 8 (2016) 16819–16840.
- [35] H. Lee, S.M. Dellatore, W.M. Miller, P.B. Messersmith, Mussel-inspired surface chemistry for multifunctional coatings, *Science* 318 (2007) 426–430.
- [36] S. He, P. Zhou, L. Wang, X. Xiong, Y. Zhang, Y. Deng, S. Wei, Antibiotic-decorated titanium with enhanced antibacterial activity through adhesive polydopamine for dental/bone implant, *J. R. Soc. Interface* 11 (2014) 20140169.
- [37] C.Y. Chien, W.B. Tsai, Poly(dopamine)-assisted immobilization of Arg-Gly-Asp peptides, hydroxyapatite, and bone morphogenic protein-2 on titanium to improve the osteogenesis of bone marrow stem cells, *ACS Appl. Mater. Interfaces* 5 (2013) 6975–6983.
- [38] N. Garrido-Mesa, A. Zarzuelo, J. Gálvez, Minocycline: far beyond an antibiotic, *Br. J. Pharmacol.* 169 (2013) 337–352.
- [39] H. Qi, Q. Chen, H. Ren, X. Wu, X. Liu, T. Lu, Electrophoretic deposition of dexamethasone-loaded gelatin nanospheres/chitosan coating and its dual function in anti-inflammation and osteogenesis, *Colloids Surf. B Biointerfaces* 169 (2018) 249–256.
- [40] A. Gauthier, A. Fisch, K. Seuwen, B. Baumgarten, H. Ruffner, A. Aebi, M. Rausch, F. Kiessling, M. Bartneck, R. Weiskirchen, F. Tacke, G. Storm, T. Lammers, M.G. Ludwig, Glucocorticoid-loaded liposomes induce a pro-resolution phenotype in human primary macrophages to support chronic wound healing, *Biomaterials* 178 (2018) 481–495.
- [41] X. Xu, L. Wang, Z. Luo, Y. Ni, H. Sun, X. Gao, Y. Li, S. Zhang, Y. Li, S. Wei, Facile and versatile strategy for construction of anti-inflammatory and antibacterial surfaces with polydopamine-mediated liposomes releasing dexamethasone and minocycline for potential implant applications, *ACS Appl. Mater. Interfaces* 9 (2017) 43300–43314.
- [42] H. Zhang, L. Xie, J. Deng, W. Zhuang, R. Luo, J. Wang, N. Huang, Y. Wang, Stability research on polydopamine and immobilized albumin on 316L stainless steel, *Regen. Biomater.* 3 (2016) 277–284.
- [43] A. López-Noriega, E. Ruiz-Hernández, E. Quinlan, G. Storm, W.E. Hennink, F.J. O'Brien, Thermally triggered release of a pro-osteogenic peptide from a functionalized collagen-based scaffold using thermosensitive liposomes, *J. Control. Release* 187 (2014) 158–166.
- [44] X. Gao, J. Song, P. Ji, X. Zhang, X. Li, X. Xu, M. Wang, S. Zhang, Y. Deng, F. Deng, S. Wei, Polydopamine-templated hydroxyapatite reinforced polycaprolactone composite nanofibers with enhanced cytocompatibility and osteogenesis for bone tissue engineering, *ACS Appl. Mater. Interfaces* 8 (2016) 3499–3515.
- [45] V. De Leo, M. Mattioli-Belmonte, M.T. Cimmarusti, A. Panniello, M. Dicarolo, F. Milano, A. Agostiano, E. De Giglio, L. Catucci, Liposome-modified titanium surface: a strategy to locally deliver bioactive molecules, *Colloids Surf. B Biointerfaces* 158 (2017) 387–396.
- [46] A.K. Gaharwar, S.M. Mihaila, A. Swami, A. Patel, S. Sant, R.L. Reis, A.P. Marques, M.E. Gomes, A. Khademhosseini, Bioactive silicate nanoplatelets for osteogenic differentiation of human mesenchymal stem cells, *Adv. Mater.* 25 (2013) 3329–3336.
- [47] F. Langenbach, J. Handschel, Effects of dexamethasone, ascorbic acid and β-glycerophosphate on the osteogenic differentiation of stem cells *in vitro*, *Stem Cell Res. Ther.* 4 (2013) 117.
- [48] G. Kaur, C. Wang, J. Sun, Q. Wang, The synergistic effects of multivalent ligand display and nanotopography on osteogenic differentiation of rat bone marrow stem cells, *Biomaterials* 31 (2010) 5813–5824.
- [49] G. Li, H. Cao, W. Zhang, X. Ding, G. Yang, Y. Qiao, X. Liu, X. Jiang, Enhanced osseointegration of hierarchical micro/nanotopographic titanium fabricated by microarc oxidation and electrochemical treatment, *ACS Appl. Mater. Interfaces* 8 (2016) 3840–3852.
- [50] M. Cheng, Y. Qiao, Q. Wang, G. Jin, H. Qin, Y. Zhao, X. Peng, X. Zhang, X. Liu, Calcium plasma implanted titanium surface with hierarchical microstructure for improving the bone formation, *ACS Appl. Mater. Interfaces* 7 (2015) 13053–13061.
- [51] N. Monteiro, A. Martins, R.A. Pires, S. Faria, N.A. Fonseca, J.N. Moreira, R.L. Reis,

- N.M. Neves, Dual release of a hydrophilic and a hydrophobic osteogenic factor from a single liposome, *RSC Adv.* 6 (2016) 114599–114612.
- [52] C. Vater, P. Kasten, M. Stiehler, Culture media for the differentiation of mesenchymal stromal cells, *Acta Biomater.* 7 (2011) 463–477.
- [53] N. Monteiro, A. Martins, R. Pires, S. Faria, N.A. Fonseca, J.N. Moreira, R.L. Reis, N.M. Neves, Immobilization of bioactive factor-loaded liposomes on the surface of electrospun nanofibers targeting tissue engineering, *Biomater. Sci.* 2 (2014) 1195–1209.
- [54] M. Chen, L. Ouyang, T. Lu, H. Wang, F. Meng, Y. Yang, C. Ning, J. Ma, X. Liu, Enhanced bioactivity and bacteriostasis of surface fluorinated polyetheretherketone, *ACS Appl. Mater. Interfaces* 9 (2017) 16824–16833.
- [55] A. Xu, L. Zhou, Y. Deng, X. Chen, X. Xiong, F. Deng, S. Wei, A carboxymethyl chitosan and peptide-decorated polyetheretherketone ternary biocomposite with enhanced antibacterial activity and osseointegration as orthopedic/dental implants, *J. Mater. Chem. B* 4 (2016) 1878–1890.
- [56] J. Vilarrasa, L.M. Delgado, M. Galofré, G. Álvarez, D. Violant, J.M. Manero, V. Blanc, F.J. Gil, J. Nart, *In vitro* evaluation of a multispecies oral biofilm over antibacterial coated titanium surfaces, *J. Mater. Sci. Mater. Med.* 29 (2018) 164.
- [57] F. Ostadhosseini, S.K. Misra, I. Tripathi, V. Kravchuk, G. Vulugundam, D. LoBato, L.E. Selmic, D. Pan, Dual purpose hafnium oxide nanoparticles offer imaging *Streptococcus mutans* dental biofilm and fight it *in vivo* via a drug free approach, *Biomaterials* 181 (2018) 252–267.
- [58] I. Chopra, M. Roberts, Tetracycline antibiotics: mode of action, applications, molecular biology, and epidemiology of bacterial resistance, *Microbiol. Mol. Biol. Rev.* 65 (2001) 232–260.
- [59] H.J. Busscher, H.C. van der Mei, G. Subbiahdoss, P.C. Jutte, J.J.A.M. van den Dungen, S.A.J. Zaat, M.J. Schultz, D.W. Grainger, Biomaterial-associated infection: locating the finish line in the race for the surface, *Sci. Transl. Med.* 4 (2012) 153rv10.
- [60] A.G. Gristina, P.T. Naylor, Q.N. Myrvik, Biomaterial-centered infections: microbial adhesion versus tissue integration, *Science* 237 (1987) 1588–1595.
- [61] A.K. Malkawi, K.H. Alzoubi, M. Jacob, G. Matic, A. Ali, A. Al Faraj, F. Almuhanha, M. Dasouki, A.M. Abdel Rahman, Metabolomics based profiling of dexamethasone side effects in rats, *Front. Pharmacol.* 9 (2018) 46.
- [62] C.M.A. van Alem, M. Boonstra, J. Prins, T. Bezhaeva, M.F. van Essen, J.M. Ruben, A.L. Vahrmeijer, E.P. van der Veer, J.W. de Fijter, M.E. Reinders, O. Meijer, J.M. Metselaar, C. van Kooten, J.I. Rotmans, Local delivery of liposomal prednisolone leads to an anti-inflammatory profile in renal ischaemia-reperfusion injury in the rat, *Nephrol. Dial. Transplant.* 33 (2018) 44–53.
- [63] F. Lühder, H.M. Reichardt, Novel drug delivery systems tailored for improved administration of glucocorticoids, *Int. J. Mol. Sci.* 18 (2017) 1836.
- [64] N.M. Vacanti, H. Cheng, P.S. Hill, J.D.T. Guerreiro, T.T. Dang, M. Ma, S. Watson, N.S. Hwang, R. Langer, D.G. Anderson, Localized delivery of dexamethasone from electrospun fibers reduces the foreign body response, *Biomacromolecules* 13 (2012) 3031–3038.
- [65] G. Ram, J. Chinen, Infections and immunodeficiency in Down syndrome, *Clin. Exp. Immunol.* 164 (2011) 9–16.
- [66] J. Zhang, L. Cai, T. Wang, S. Tang, Q. Li, T. Tang, S. Wei, J. Qian, J. Wei, J. Su, Lithium doped silica nanospheres/poly(dopamine) composite coating on polyetheretherketone to stimulate cell responses, improve bone formation and osseointegration, *Nanomedicine* 14 (2018) 965–976.
- [67] X. Zhou, W. Feng, K. Qiu, L. Chen, W. Wang, W. Nie, X. Mo, C. He, BMP-2 derived peptide and dexamethasone incorporated mesoporous silica nanoparticles for enhanced osteogenic differentiation of bone mesenchymal stem cells, *ACS Appl. Mater. Interfaces* 7 (2015) 15777–15789.
- [68] L. Li, G. Zhou, Y. Wang, G. Yang, S. Ding, S. Zhou, Controlled dual delivery of BMP-2 and dexamethasone by nanoparticle-embedded electrospun nanofibers for the efficient repair of critical-sized rat calvarial defect, *Biomaterials* 37 (2015) 218–229.